ARL-TR-94-18

Copy No. 58

Detection and Localization Using Two Horizontally Separated Vertical Line Arrays

Technical Report under Contract N00039-91-C-0082
TD No. 01A1030, Spatial and Temporal Signal and Noise Analysis

Evan K. Westwood

Applied Research Laboratories
The University Of Texas At Austin
P. O. Box 8029 Austin, TX 78713-8029

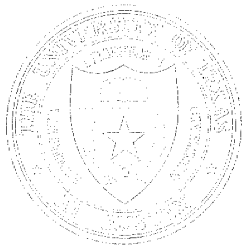

17 October 1994

Technical Report

Approved for public release; distribution is unlimited.

Destruction Notice: - For classified documents, follow the procedures in DoD Manual 5200.22-M, Industrial Security Manual. For unclassified, limited distribution documents, destroy by any method that will prevent disclosure of contents or reconstruction of the document.

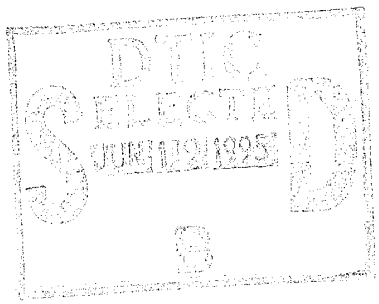

Prepared for:
Naval Command, Control, and Ocean Surveillance Center
RDT&E Division
San Diego, CA 92152-5000

Monitored by:
Space and Naval Warfare Systems Command
Department of the Navy
Arlington, VA 22245-5200

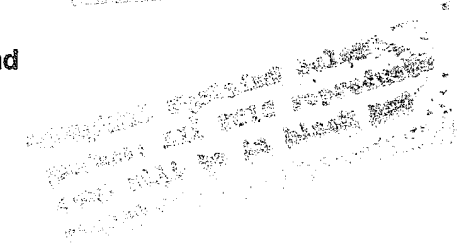

DISCLAIMER NOTICE

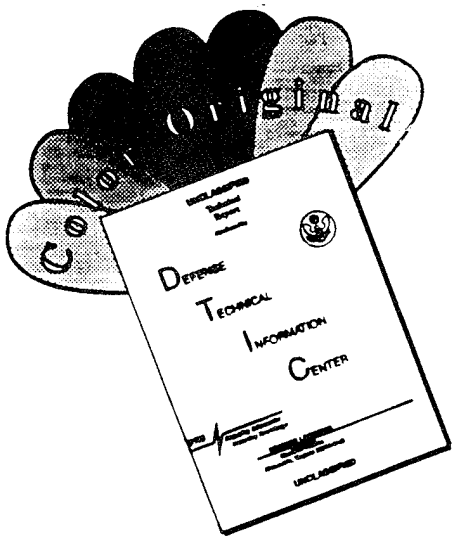

THIS DOCUMENT IS BEST QUALITY AVAILABLE. THE COPY FURNISHED TO DTIC CONTAINED A SIGNIFICANT NUMBER OF COLOR PAGES WHICH DO NOT REPRODUCE LEGIBLY ON BLACK AND WHITE MICROFICHE.

REPORT DOCUMENTATION PAGE

Form Approved
OMB No. 0704-0188

1. AGENCY USE ONLY (Leave blank)	2. REPORT DATE	3. REPORT TYPE AND DATES COVERED
	17 Oct 94	technical

4. TITLE AND SUBTITLE

Detection and Localization Using Two Horizontally Separated Vertical Line Arrays, Technical Report under Contract N00039-91-C-0082, TD No. 01A1030, Spatial and Temporal Signal and Noise Analysis

5. FUNDING NUMBERS

N00039-91-C-0082,
TD No. 01A1030

6. AUTHOR(S)

Westwood, Evan K.

7. PERFORMING ORGANIZATION NAMES(S) AND ADDRESS(ES)

Applied Research Laboratories
The University of Texas at Austin
P.O. Box 8029
Austin, Texas 78713-8029

8. PERFORMING ORGANIZATION REPORT NUMBER

ARL-TR-94-18

9. SPONSORING/MONITORING AGENCY NAME(S) AND ADDRESS(ES)

Naval Command, Control, and Ocean Surveillance Center
RDT&E Division
San Diego, California 92152-5000

Space and Naval Warfare Systems Command
Department of the Navy
Arlington, VA 22245-5200

10. SPONSORING/MONITORING AGENCY REPORT NUMBER

11. SUPPLEMENTARY NOTES

12a. DISTRIBUTION/AVAILABILITY STATEMENT

Approved for public release; distribution is unlimited.

12b. DISTRIBUTION CODE

13. ABSTRACT (Maximum 200 words)

A method for ASW detection and localization using two horizontally separated vertical line arrays is applied to the TAGEX 87 deep water data set. The method consists of beamforming the two vertical arrays and crosscorrelating the beamformer outputs. Application of the method to a 5 hr time period during which several ships pass near the two arrays results in clear detections of two ships. A correlagram fitting procedure is used to localize the ships, and simulated beam-cross-beam correlagrams agree well with the measured data. Simulated signals from quiet sources are injected into the measured data, and detectability as a function of range and source level is investigated.

14. SUBJECT TERMS

detection
localization
beamforming
crosscorrelation
vertical line array
TAGEX 87
deep water

15. NUMBER OF PAGES

51

16. PRICE CODE

17. SECURITY CLASSIFICATION OF REPORT	18. SECURITY CLASSIFICATION OF THIS PAGE	19. SECURITY CLASSIFICATION OF ABSTRACT	20. LIMITATION OF ABSTRACT
UNCLASSIFIED	UNCLASSIFIED	UNCLASSIFIED	SAR

NSN 7540-01-280-5500

Standard Form 298 (Rev. 2-89)
Prescribed by ANSI Std. 239-18
298-102

This page intentionally left blank.

TABLE OF CONTENTS

1. **INTRODUCTION** 1

2. **CLOCK SYNCHRONIZATION AND ARRAY LOCALIZATION** 3

   2.1 Experiment Geometry 3

   2.2 Clock Synchronization 3

3. **VERTICAL NOISE STRUCTURE** 9

4. **BEAM-CROSS-BEAM CORRELATIONS** 17

   4.1 Algorithm 17

   4.2 Beam-Cross-Beam Correlagrams of Recorded Data 19

   4.3 Analysis of Ship 1 21

   4.4 Localization and Simulation of Ship 2 24

   4.5 Variation of Beam-Cross-Beam Parameters 28

   4.6 Sector-Focused Beam Patterns 29

5. **SIMULATED DETECTABILITY OF QUIET SOURCES** 35

   5.1 Stationary Source with Increasing Level 36

   5.2 Moving Source at Constant Level 37

   5.3 Sonar Equation Analysis of Simulated Detections 40

6. **SUMMARY AND CONCLUSIONS** 43

REFERENCES 45

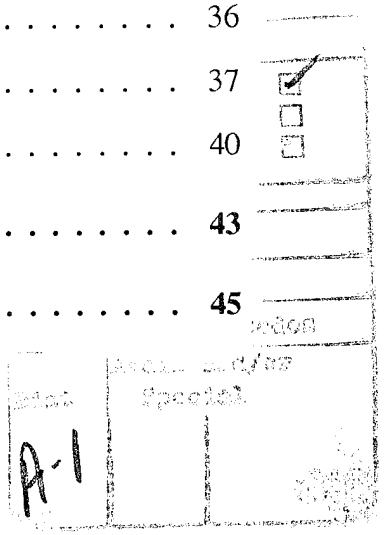

This page intentionally left blank.

LIST OF FIGURES

2.1 Array configuration for the TAGEX 87 V1 and V2 vertical arrays. 4

2.2 Vertical correlagrams between the bottom and top receivers of (a) V1 and (b) V2 5

2.3 Source track relative to (a) V1 and (b) V2 that produced the best fit correlagrams shown in Fig. 2.2.. 6

2.4 The two possible configurations for V1, V2, and the source track obtained by combining Fig. 2.3(a) and (b) 7

2.5 Comparison of (a) measured and (b) simulated inter-array correlagrams using the bottom receivers of each array. 8

3.1 ABF beamgrams at (a) V1 and (b) V2 for the frequency band 75–100 Hz . . . 10

3.2 ABF beamgrams at (a) V1 and (b) V2 for the frequency band 100–140 Hz . . . 11

3.3 Simulated R–θ function for the TAGEX 87 environment 13

3.4 Eigenrays at ranges of 10, 40, and 80 km 15

4.1 Procedure for beam-cross-beam correlation 18

4.2 Beam-cross-beam correlagram for the entire 5 hr time period 20

4.3 Simulated correlagram produced by the ship track derived in Sec. 2. 23

4.4 Source track localization of ship 2 25

4.5 Simulated correlagram for the derived source track of ship 2 26

4.6 Simulated correlagram of the superposed signals from ships 1 and 2 27

4.7 Uninterpolated portion of the beam-cross-beam correlagram of Fig. 4.2. . . . 28

4.8 Beam-cross-beam correlagram formed by crosscorrelating only beams steered at the same angle (the diagonal of the beam pair matrix) 29

4.9 Beam-cross-beam correlagram formed by steering beams from 16°–90° 30

4.10 Broadband beam pattern synthesized using the ISM algorithm for V2 for a passband of 0°–30° 31

4.11 Beam-cross-beam correlagram produced by steering eight pencil beams at V1 and one sector beam at V2 33

5.1 Source-receiver geometry for the stationary source with increasing level 36

5.2 Beam-cross-beam correlagrams using (a) ABF and (b) CBF for a simulated source at 3.6 km 37

5.3 Source-receiver geometry for the constant-level source moving at a speed of 2.5 m/s 39

5.4 Beam-cross-beam correlagram for the 125 dB source moving along the track shown in Fig. 5.3 39

1. INTRODUCTION

This report evaluates a method for passive acoustic detection and localization that uses two horizontally separated vertical line arrays (VLAs) as the sensor configuration. The method is applied to data recorded at two VEDABS arrays during the TAGEX 87 experiment. The vertical arrays were bottom-moored in deep water 3.8 km apart and were cut for frequencies near 75 Hz. The signal processing scheme applied to the data consists of beamforming the two vertical arrays separately, crosscorrelating selected pairs of beams, and combining the multiple correlations into a single display.

The basic principle behind the 2-VLA sensor configuration is that the vertical aperture of each array can be used to reject the distant shipping noise that arrives from low grazing angles. By steering beams in directions steeper than the distant shipping noise, one can realize low beam noise while attempting to detect sources at short and medium ranges. Crosscorrelating the vertical beams across a horizontal aperture then provides azimuthal information on the source track. Ideally, the quiet vertical beams should result in "quiet" correlagrams that will be sensitive to low level sources at short and medium ranges. An important issue regarding the effectiveness of the 2-VLA configuration is the coherence of the noise and signal fields across the horizontal aperture.

The report is organized in the following manner. In Sec. 2 the array configuration is summarized, and the methods for synchronizing the two arrays' independent clocks and for finding the separation between the two arrays are presented. Section 3 contains an analysis of the vertical noise directionality structure measured at the two arrays. In Sec. 4 the signal processing algorithm is reviewed and applied to the measured data. Two passing ships are localized using a correlagram fitting procedure, a broadband ray model (see Refs. 1 and 2) is used to simulate the signals produced by the two ships, and the simulated data are processed according to the algorithm as well. The ray model is used again in Sec. 5 to simulate a quiet submarine-like source at short range. The simulated signals at various source levels are added to the measured data, and the detectability of quiet sources using the 2-VLA configuration is evaluated. Section 6 contains the conclusions drawn from this work.

This page intentionally left blank.

2. CLOCK SYNCHRONIZATION AND ARRAY LOCALIZATION

2.1 Experiment Geometry

The TAGEX 87 experiment was conducted in April 1987 at a deep-water site about 500 km east of the northern Florida coast. Two 26-element bottom-moored vertical line arrays (VLAs) were deployed in 4600 m deep water. The array configurations are illustrated in Fig. 2.1. The first array, V1, consists of 24 hydrophones spaced 10 m apart, plus two hydrophones spaced 1.5 m apart at the bottom of the array. The second array, V2, consists of two identical 70 m subarrays separated by 128 m. Each subarray is made up of seven hydrophones spaced at 10 m, plus six hydrophones spaced 2 m apart surrounding the subarray's middle element. The bottom elements of V1 and V2 are 40 m and 25 m off the ocean bottom, respectively. According to the deployment ship logs, the two arrays were placed 3.8 km apart, and V2 was located at a bearing of 88.9°E of N from V1. The two arrays were independent of one another, and thus the clocks used for data recording were not synchronized.

2.2 Clock Synchronization

In order to process the two arrays simultaneously, it is necessary to determine the array separation and the offset between the two clocks. Before proceeding with the synchronization technique, which relies heavily on broadband crosscorrelation, the processing parameters used to produce correlagrams are summarized. The recorded time series are sampled at a rate of 300 Hz and broken into segments of 4000 data points plus 96 zeros.* Successive segments are overlapped 50%, which means each segment consists of 13.33 s of data, and successive segments begin 6.67 s apart. The data segments are passed through a discrete Fourier transform (implemented with a fast Fourier transform (FFT)) to the frequency domain, where the cross-spectra are formed. Tones are removed, using a pre-whitening algorithm known as

*Zero padding allows an even number of segments to fill up the 2 min processing interval used in the analog-digital conversion process.

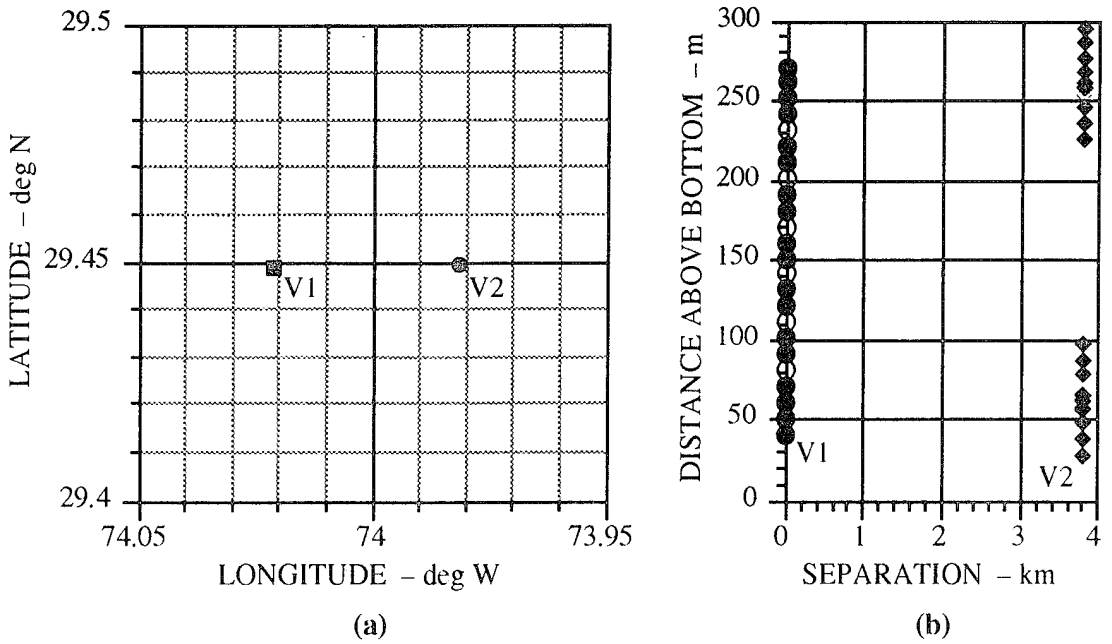

FIGURE 2.1 Array configuration for the TAGEX 87 V1 and V2 vertical arrays: (a) reported array locations, and (b) array geometries. Solid symbols denote array elements used to obtain the beamforming results in this report. (AS-94-1051)

SCOT weighting, before inverse FFTing to obtain the correlation coefficient as a function of delay time. The correlation values as a function of delay time and recording time (or segment number) are plotted as a gray shade image known as a correlagram.

The clock offset is found by crosscorrelating receivers from the two arrays during a time period in which a loud ship passes by. The signal from the ship should produce a strong trace on a correlagram when the correct clock offset is applied. First, the inter-array crosscorrelation is performed as though the two clocks were synchronized, i.e., FFTs from the two receivers are processed with no segment offset. The resulting correlagram exhibits no traces, indicating that the assumed clock offset of zero is incorrect. Next, the correlation is performed with V2 delayed by one data segment, corresponding to the assumption that V2's clock is 6.67 s fast compared to V1's. Again, the correlagram exhibits no trace. A trace is finally found when V2 is delayed *two* data segments. (The correlagram trace will be shown in Fig. 2.5(a) after the exact clock offset is determined.) It is concluded that V2's clock is 13.33±6.67 s fast compared to V1's. The exact clock offset can only be determined after the ship track relative to the two arrays is known.

In order to determine the array separation, vertical crosscorrelations are performed using the top and bottom receivers of the two arrays (see Fig. 2.2). The strong trace in each correlagram is produced by correlation between the direct path at the bottom and top receivers. The

"DxD" (for "direct-cross-direct") correlation traces reach their maximum time delay at about the same time, indicating the ship reached its closest point of approach (CPA) relative to the two arrays simultaneously.

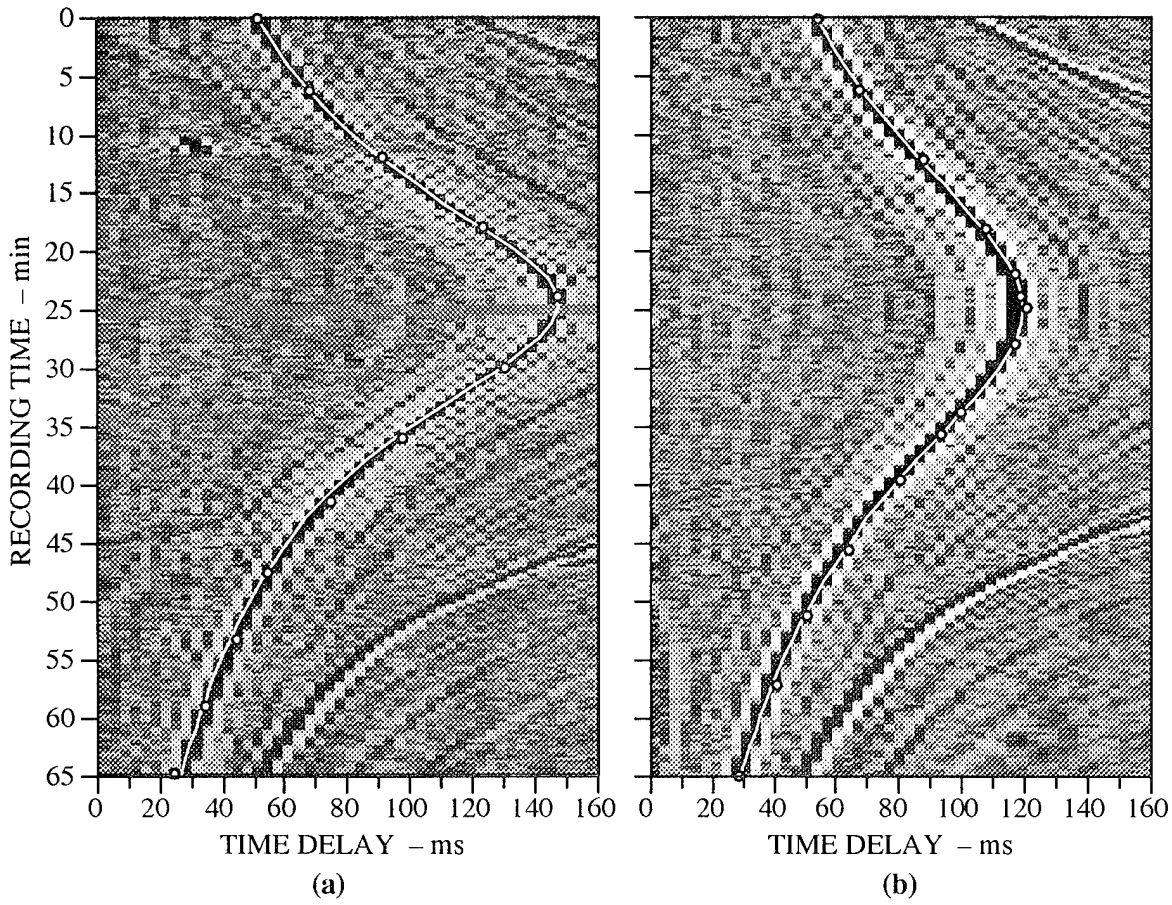

FIGURE 2.2 Vertical correlagrams between the bottom and top receivers of (a) V1 and (b) V2. The primary trace is the direct-cross-direct (DxD). White dots are points used in the source localization algorithm. The white lines are the correlation traces produced by the best fit source track. (AS-94-1052)

The ship track relative to each array is found from the vertical correlagrams in Fig. 2.2 using a correlagram fitting technique, which is now described. Sample points taken from the DxD trace are used as inputs to a non-linear optimization algorithm that finds the constant velocity, straight line source track that produces a best fit to the correlagram trace. The simulated correlagram traces produced by the candidate source tracks are found by tracing rays through the actual sound velocity profile measured in the area. The points from the DxD traces used in the source track localization procedure are indicated by white dots in Fig. 2.2, and the best fits to the traces are indicated by white lines. It is evident that the correlation trace fits are excellent, which implies that the estimate of the source track is accurate.

The source tracks that produce the best fits are shown in Fig. 2.3. The tracks have been plotted horizontally by default since no azimuthal information is provided by the vertical aperture crosscorrelation. The ranges of the ship at the CPAs are 0.8 and 4.6 km at V1 and V2, respectively. The close agreement in the source velocities from the two independent localizations, 7.42 m/s at V1 and 7.43 m/s at V2, is another indication that the localizations are accurate.

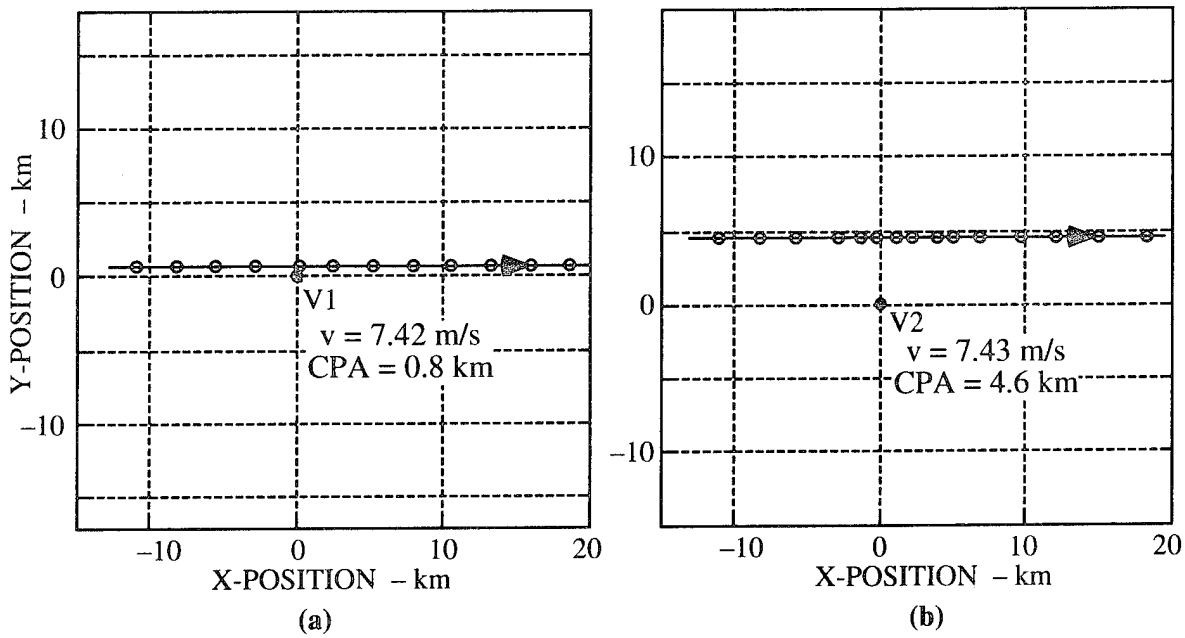

FIGURE 2.3 Source track relative to (a) V1 and (b) V2 that produced the best fit correlagrams shown in Fig. 2.2. Since the correlations are across a vertical aperture, no azimuthal information is available, and the tracks have been plotted horizontally. The closest point of approach (CPA) and source velocity (v) are indicated on the maps. (AS-94-1053)

Once the ship has been localized relative to each array individually over the same time period,* the relative positions of the two arrays are determined by placing the source track maps of Fig. 2.3 on top of each other so that the source tracks themselves overlie one another. As illustrated in Fig. 2.4, two different configurations are possible: the two arrays can be on the same side or on opposite sides of the source track. The distance between V1 and V2 is 3.8 km in the first case and 5.3 km in the second case. The ambiguity exists because the source track is linear: any curvature in the source track would break the side-to-side symmetry. Using only the current ship passage, it is not possible to determine which of the two configurations in Fig. 2.4 is correct.

*Recall that the two clocks have been synchronized to within ±6.67 s, during which time the ship travels (assuming a velocity of 7.42 m/s) a distance of about 50 m. Such an offset between the two tracks will not significantly affect the computation of the array separation.

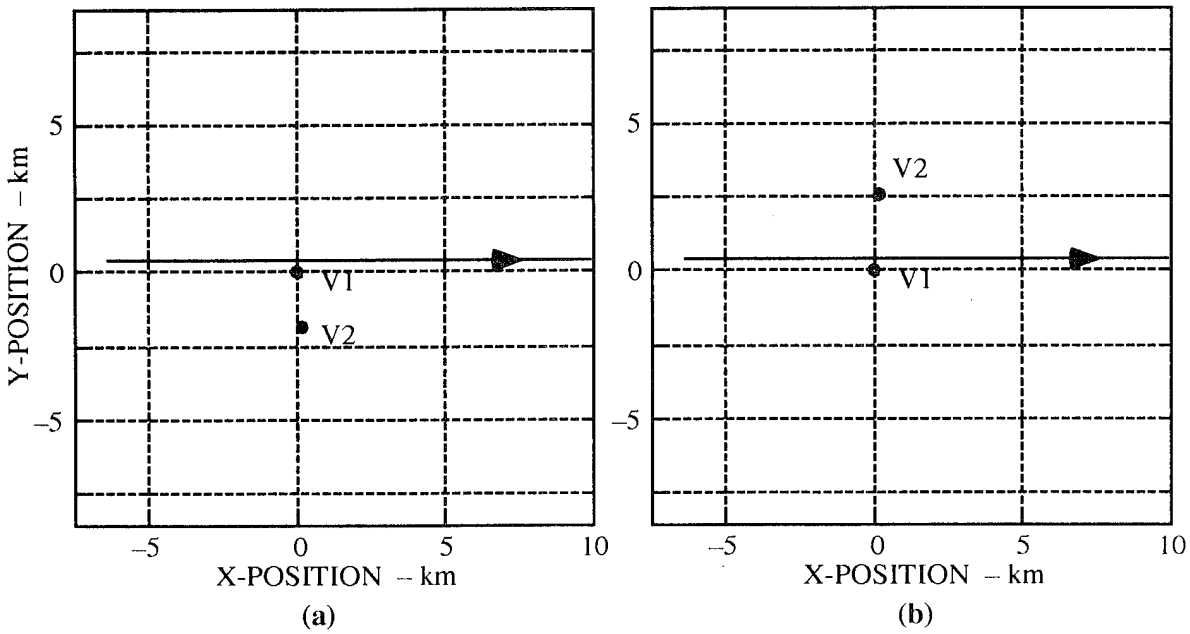

FIGURE 2.4 The two possible configurations for V1, V2, and the source track obtained by combining Fig. 2.3(a) and (b): (a) V1 and V2 on the same side of the source track, and (b) V1 and V2 on opposite sides of the source track. (AS-94-1054)

The derived configurations in Fig. 2.4 *do* allow us to model the inter-array correlagram and to determine the exact inter-array clock offset. Figure 2.5 shows a comparison between the measured and simulated inter-array correlagrams (using the bottom receivers of each array). The measured correlagram was shifted horizontally to match the simulation because the exact clock offset between the two arrays was still undetermined. The amount of time delay shift is –1.15 s, which, when added to the two-segment (13.33 s) offset discussed earlier, makes the total clock offset 12.18 s. Note that modeled inter-array correlagrams using the two configurations shown in Fig. 2.4 are identical due to the left-right symmetry of the two-array system.

Although the possible array separation of 3.8 km is identical to the figure derived from the deployment ship log, the correct separation between the two arrays can be determined from acoustic measurements only by examining a second ship passage. In the 5 hr time period examined, a second ship CPA occurs at time 212 min from the beginning of the period. Because the ship reaches its CPA at a much longer range (derived to be around 30 km) and the noise from the first ship is still present, the single receiver crosscorrelations do not detect the second ship. In Sec. 4 the crosscorrelation of vertical beams is used to detect the second ship, and in Sec. 4.4 the ship is localized, and, in the process, the array separation is determined to be 3.8 km rather than 5.3 km.

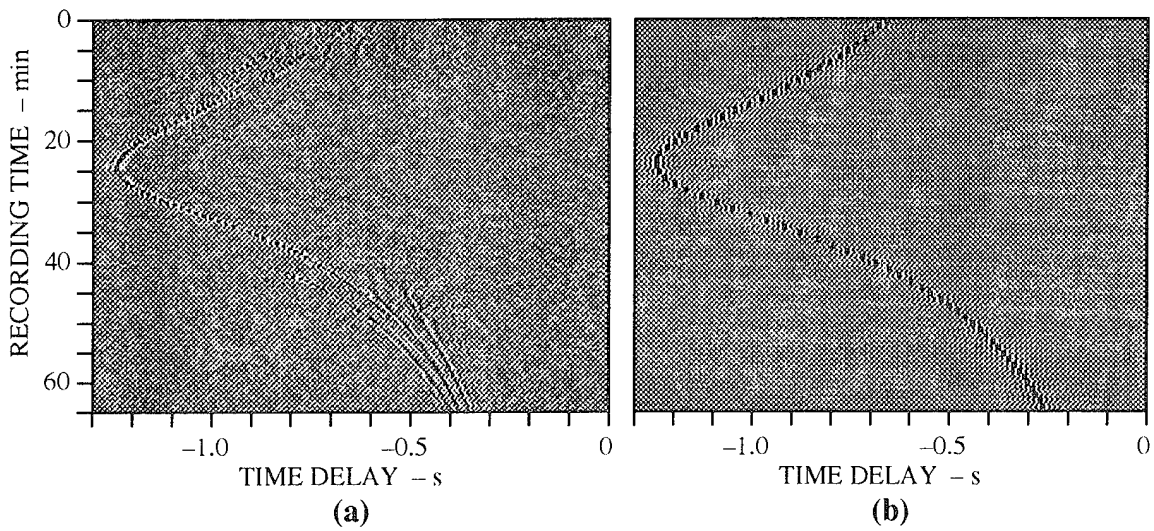

FIGURE 2.5 Comparison of (a) measured and (b) simulated inter-array correlagrams using the bottom receivers of each array. The measured correlagram was shifted horizontally the amount required to match the simulation. (AS-94-1055)

To summarize, the gross clock offset (to within ±6.67 s) is first found by performing inter-array correlagrams during a loud ship passage. Vertical correlagrams are then used to localize the ship relative to the individual arrays. Two possible array separations are derived by merging the two maps so that the ship tracks overlie. The exact clock offset is determined by simulating the inter-array correlagram and shifting the data in time delay so that the DxD traces match. Finally, as will be shown in Sec. 4, resolution of the array separation ambiguity is achieved by examining a second, more distant ship passage. Knowledge of the clock offset and array separation allow simultaneous processing of the two arrays.

3. VERTICAL NOISE STRUCTURE

Before the two vertical arrays are processed simultaneously, the vertical noise directionality measured at the two arrays separately is examined. A 5 hr time period of the TAGEX 87 data set is chosen, part of which was used in Sec. 2 to localize the arrays and during which two ships reach their CPAs at ranges of approximately 2 and 30 km. The vertical arrays are beamformed, and imaged displays of beamformer output versus vertical arrival angle and recording time, which are called "beamgrams," are produced. The beamgrams are expected to exhibit time-varying traces produced by the ray arrivals from the passing ships, as well as a constant, broad peak centered about the horizontal (broadside) direction produced by energy arriving at small grazing angles from distant shipping. The features of the beamgrams produced by ships are compared to ray model predictions for the vertical ray arrival structure of an acoustic source as a function of range.

Noise directionality measurements are obtained using an adaptive beamformer (ABF) based on the implementation described in Ref. 3. In order to reduce processing time and storage space, 18 receivers from each array are used [see the solid symbols in Fig. 2.1(b)]. The white noise gain constraint of the ABF algorithm, which is designed to make the beamformer more tolerant of errors in element position and calibration, is set to a value of –6 dB. The ABF processor requires estimates of the cross-spectral matrix (CSM). In forming the CSMs from the receiver spectra, time averaging over 1 min intervals and frequency averaging over 1 Hz bands are performed. Beams are steered at 181 steering angles (evenly spaced in sine of the grazing angle) from end-fire to end-fire.

The ABF beamgrams, averaged from 75–100 Hz and from 100–140 Hz over a 4 hr 27 min interval,* are shown in Figs. 3.1 and 3.2, respectively. The traces in the beamgrams are labeled according to the number of ocean traversals of the eigenrays that produce them. The CPA of ship 1 occurs simultaneously at V1 and V2 near time 30 min and produces direct-path (1-traversal) traces that reach maximum vertical angles of 80° at V1 and 40° at V2. The steeper angle at V1 simply reflects the fact that the ship passed closer to V1 than to V2. The

*The final 33 min of the intended 5 hr time period were inadvertently omitted.

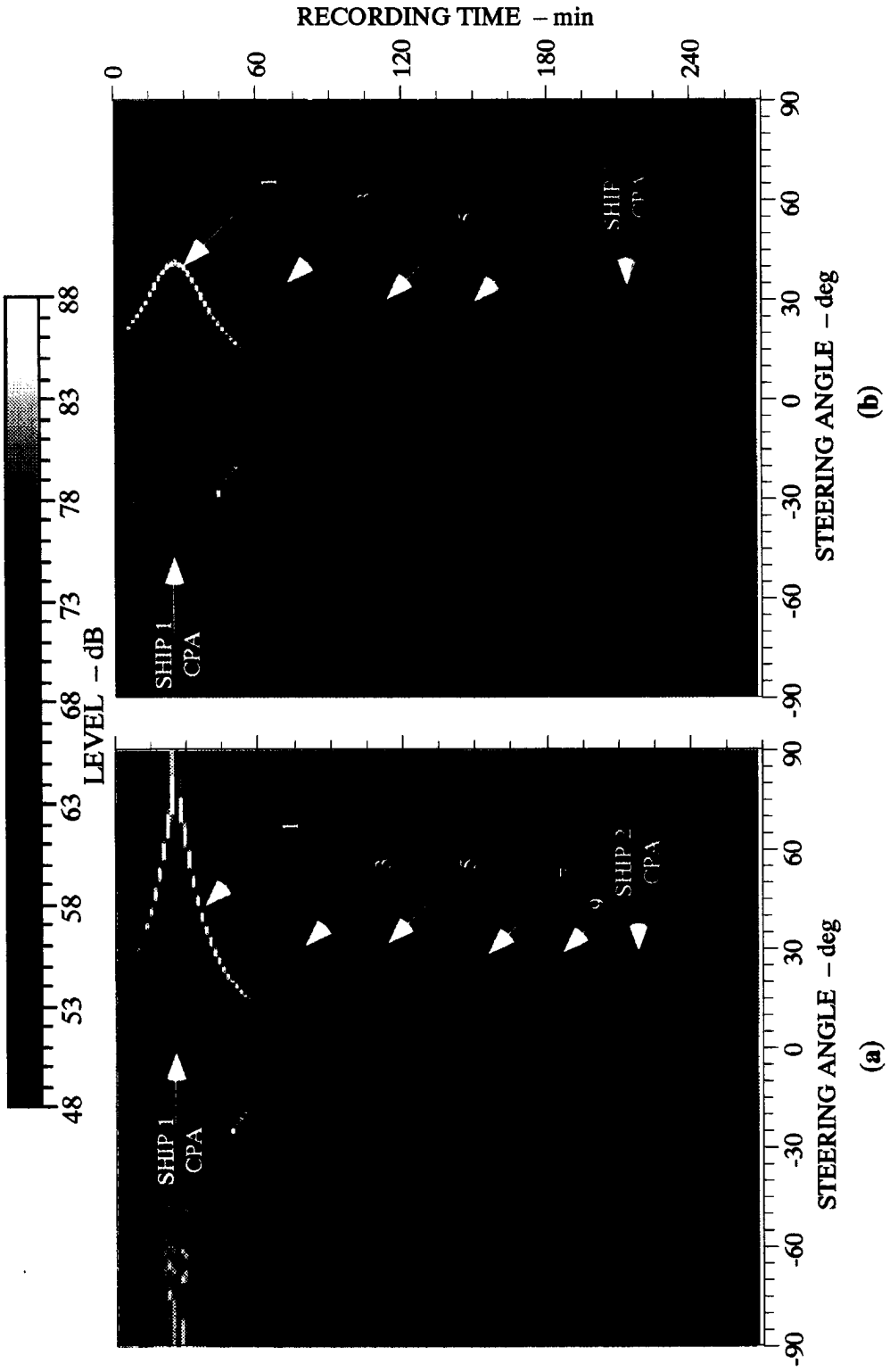

FIGURE 3.1 ABF beamgrams at (a) V1 and (b) V2 for the frequency band 75–100 Hz. (AS-94-1057)

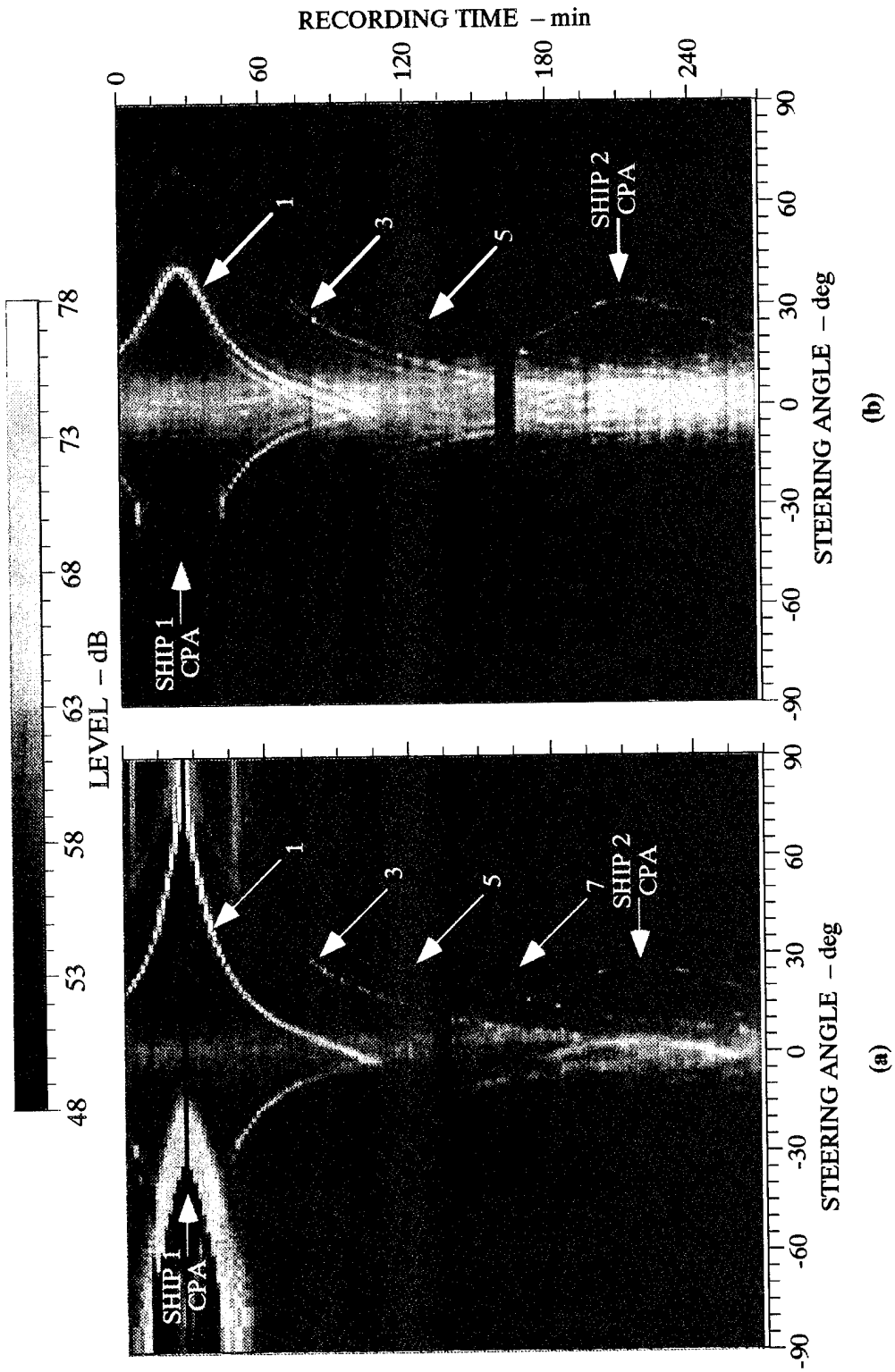

FIGURE 3.2 ABF beamgrams at (a) V1 and (b) V2 for the frequency band 100–140 Hz. (AS-94-1057)

CPA of ship 2 occurs near time 215 min at V1 and about 5 min earlier at V2. The trace, which will be shown in Sec. 4.4 to be produced by 3-traversal rays, reaches maximum grazing angles of 25° at V1 and 32° at V2, indicating a shorter CPA range relative to V2. The following observations are made regarding the structure of the vertical beamformer outputs in Figs. 3.1 and 3.2:

1. As the first ship's range increases, traces produced by eigenrays with successively more ocean traversals are observed, and each trace moves toward shallower grazing angles.
2. A given trace disappears beyond a certain range where the eigenray no longer reaches the receiver depth because of refraction in the water column. For example, the direct path eigenray disappears at time 105 min.
3. As the number of ocean traversals increases, eigenrays (and thus the corresponding beamgram traces) are weaker because they have longer path lengths and experience more reflection loss at the bottom.
4. At short ranges the bottom-penetrating eigenray (at negative steering angles) arrives at slightly steeper angles than the direct eigenray. As the range increases and the rays do not penetrate as deeply into the bottom, the rays arrive at angles symmetric about 0° grazing.
5. The background noise is concentrated in a region around broadside, between approximately ±15°. The horizontal component of the noise is produced by energy from distant shipping that has traversed the ocean many times. The tendency of the noise to concentrate about horizontal as the range increases may be seen from the traces produced by the first ship: by the end of the time period, when the ship is over 100 km away, most of its energy has blended into the background noise.

The ray arrivals observed on the vertical beamgrams of Figs. 3.1 and 3.2 may be simulated by using a ray model (see Refs. 1 and 2) to produce plots of the horizontal range R versus vertical arrival angle θ at the receiver for a variety of different ray paths. Such plots are commonly referred to as R–θ functions. Figure 3.3 shows the R–θ plot for the TAGEX 87 environment, where the ray arrivals are imaged according to their strength (at a frequency of 60 Hz) in dB. For each range the maximum ray magnitude is normalized to 0 dB. The color scale is chosen to cover 60 dB in order to show the detailed structure of the ray arrivals; in the noisy ocean one would expect to observe 30 dB or less of dynamic range.

The eigenray structure observed in the simulated R–θ plot of Fig. 3.3 is in good agreement with the measured beamgrams of Figs. 3.1 and 3.2. The R–θ plot also shows that a single

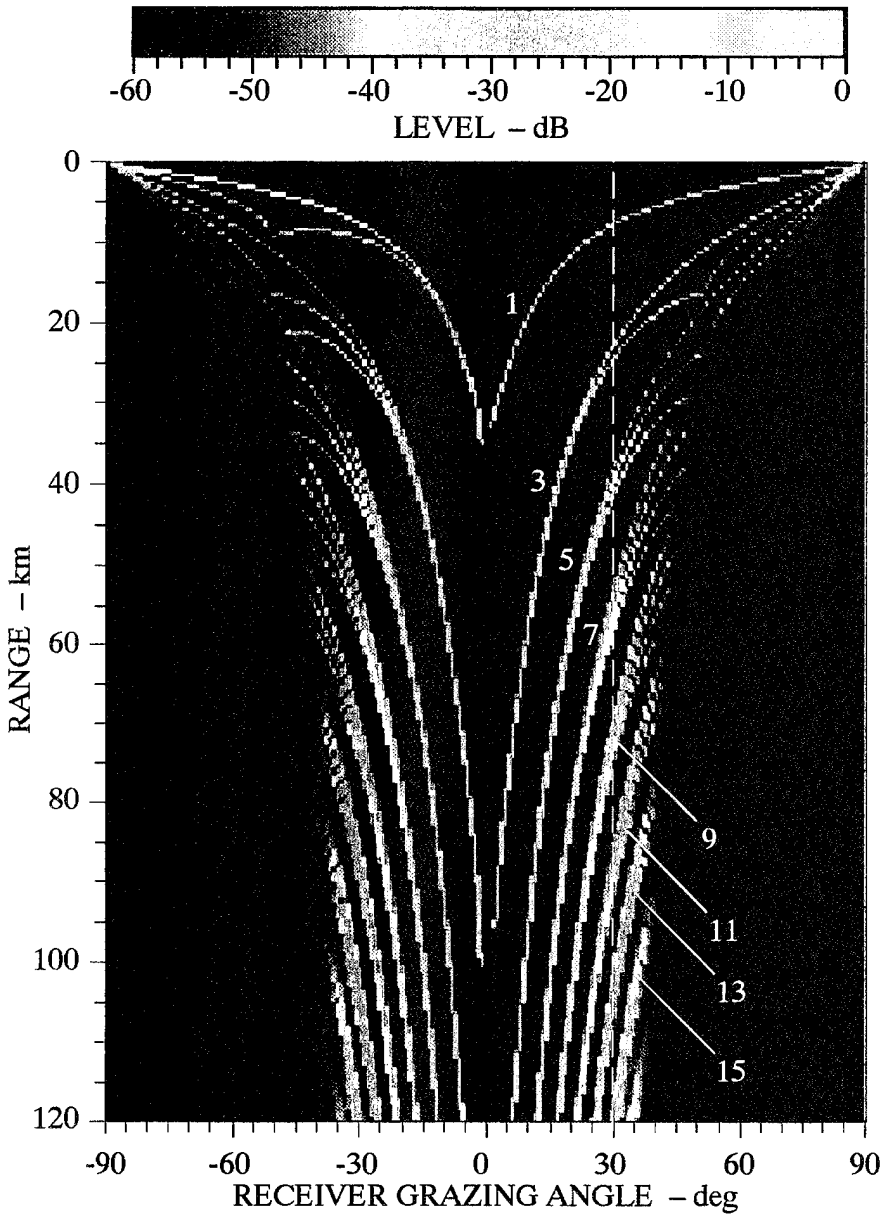

FIGURE 3.3 Simulated R–θ function for the TAGEX 87 environment. Labels indicate the number of ocean traversals of the ray arrivals. (AS-94-1058)

trace at long range and shallow angles splits into multiple traces at shorter ranges and steeper angles. The multipaths for a given number of ocean traversals differ by the number of times they reflect off the ocean bottom versus the number of times they penetrate into the bottom. As the range increases the rays turn at shallower depths, and the ray angles of all the multipaths converge. It is also interesting to note that, as the range increases, the difference in strength between adjacent multipaths (those having n and $n + 2$ traversals) decreases. The reasons are: (1) the path length difference between such rays decreases as the range increases, and (2) the loss due to an additional bottom interaction decreases as the range increases.

Figure 3.4 illustrates several of the eigenray paths that appear in the measured beamgrams and the simulated R–θ plot. Eigenrays within 30 dB of the strongest ray are plotted for ranges of 10 km (red), 40 km (blue), and 80 km (green). At 10 km, eigenrays with 1 and 3 ocean traversals exist; at 40 km, rays with 3, 5, and 7 traversals exist (the direct ray is cut off); and at 80 km, rays having from 3, 5, 7, 9, and 11 traversals exist (although the 3-traversals are close to cutoff).

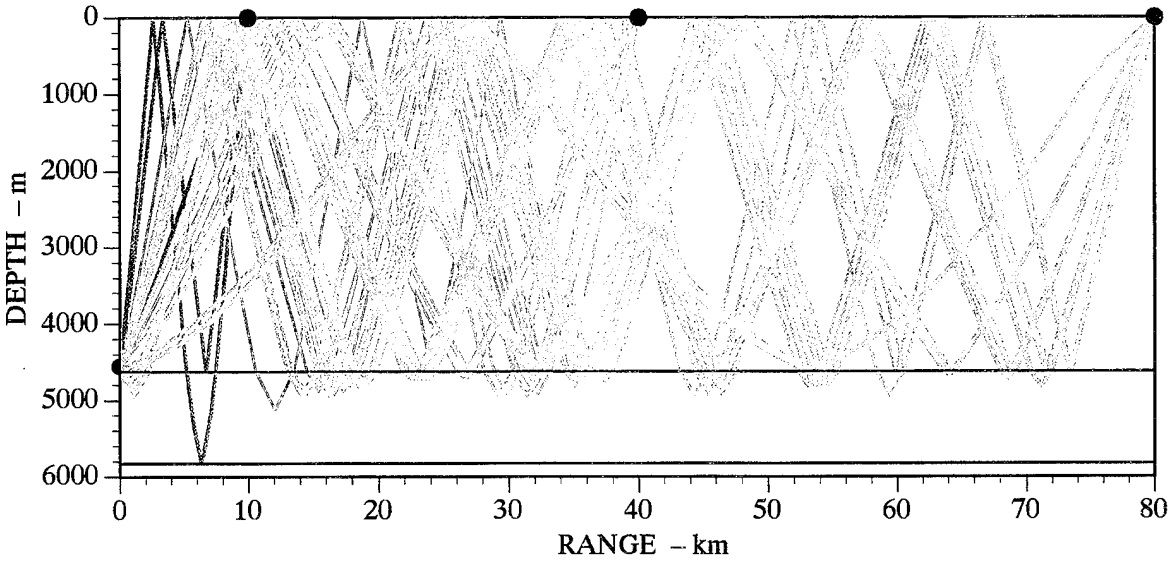

FIGURE 3.4 Eigenrays at ranges of 10, 40, and 80 km. (AS-94-1059)

This page intentionally left blank.

4. BEAM-CROSS-BEAM CORRELATIONS

4.1 Algorithm

The data processing scheme that appears to be best suited for the case of two horizontally separated vertical arrays consists of forming vertical beams with the two arrays and crosscorrelating the complex beamformer outputs. The basic procedure is illustrated in Fig. 4.1. The objective is to achieve gain against the horizontally arriving, shipping induced noise by beamforming the vertical arrays, while obtaining azimuthal discrimination from the horizontal separation of the arrays. The two most daunting issues associated with the scheme are: (1) how to decide which vertical beams to form and which beam pairs to crosscorrelate, and (2) how to reduce and display the large amount of data that is produced.

Factors affecting the first issue are:

1. The number of elements N_e in each of the arrays: as N_e increases, the beams become narrower and more beams must be steered to cover a given interval of vertical angles.
2. The vertical structure of the ambient noise at the array site. For example, in deep water the ambient noise from distant sources typically arrives in some interval centered about 0° grazing angle. In order to detect short- and intermediate-range sources, vertical beams need not be steered at angles in that interval.
3. The horizontal separation of the two vertical arrays compared to the water depth. For large horizontal separations and nearby sources, energy from a source of interest can appear on widely different vertical beams, which makes it necessary to correlate a large number of beam pairs. On the other hand, if the two arrays are close together and sources are at ranges that are large compared to the separation, the vertical arrival angles at the two arrays are almost the same, and only beams steered at the same vertical angle need be crosscorrelated.
4. The type of beamforming used. Adaptive beamformers (ABFs) generally have narrower beamwidths than conventional beamformers (CBFs), and thus would require more beams to be steered. An alternative to ABF and CBF is to design a beam pattern that passes energy from the angular region of interest while rejecting energy from

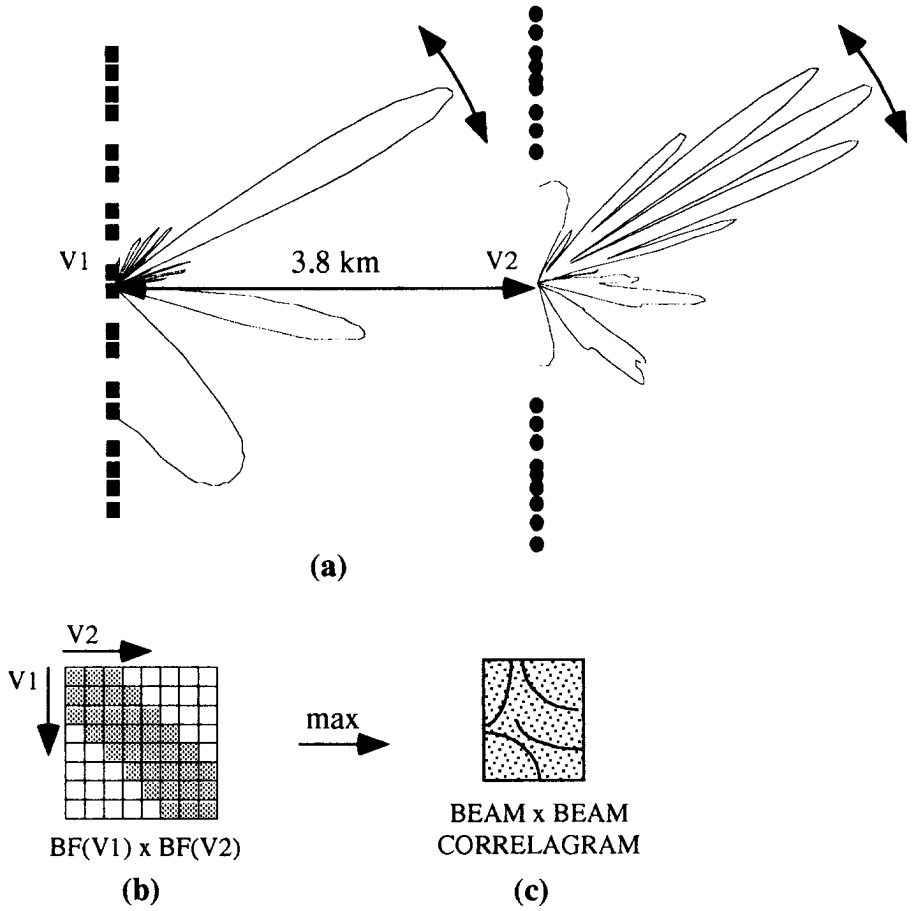

FIGURE 4.1 Procedure for beam-cross-beam correlation: (a) illustration of beam patterns at V1 and V2, (b) beam pair matrix, where beam pairs up to two positions off the main diagonal have been shaded, and (c) the final correlagram display obtained by taking the maximum values over all the correlagrams are taken. (AS-94-1060)

other angles. For a vertical array a sector beam pattern that passes energy between, say, 15° and 90° could be useful. The advantage of such a "sector beamformer" is that only one beam would need to be formed at each array, and only one crosscorrelation would need to be performed. The disadvantage of the sector beamformer is that the beam pattern nulls are not as deep as those obtained using CBF and ABF.

A convenient way to address the second issue is to parametrize the number of correlations by forming a matrix of beam pairs, where element *i,j* corresponds to the correlation between beam *i* from array 1 and beam *j* from array 2, and to specify which part of the matrix is to be computed. For arrays with similar numbers of elements, it makes sense to form equal numbers of beams, which results in a square "beam pair matrix." The like-beam correlations, that is, those on the diagonal of the beam pair matrix, are almost always of interest. In this report, additional sets of beams are specified by the number of diagonals off the main diagonal

of the beam pair matrix. For example, using "up to two off-diagonals" of the beam pair matrix [see Fig. 4.1(b)] means using the main diagonal plus the two neighboring diagonals above and below. For N_B beams, the total number of correlations required to compute N_D off-diagonals is

$$N_C = N_B + 2\sum_{k=1}^{N_D}(N_B - k) \quad . \tag{4.1}$$

The issue of displaying the output of the beam-cross-beam processor concerns finding a method for merging the multiple correlagrams that preserves the signal traces. In addition, it would be desirable to be able to find out which beams produce the traces that appear on the final display. In this report perhaps the simplest (and most efficient) method for merging the multiple correlagrams is used: for each time delay pixel, the maximum absolute value of the correlation in all the computed correlagrams is entered into the final correlagram output. Along with the final correlagram, two tables are produced that contain, for each pixel in the correlagram, the beam angles that produced the maximum value found. Thus the vertical beams that detected a given trace in the merged correlagram can be identified.

4.2 Beam-Cross-Beam Correlagrams of Recorded Data

The beam-cross-beam correlation procedure is applied to the same 5 hr period from the TAGEX 87 data set analyzed previously. For the initial attempt CBF is used to steer eight beams from grazing angles of 0°–30°, evenly spaced in sin θ, over the frequency band 10–140 Hz. (Beams are not steered past 30° because the sources of interest are the two dominant ships.) In forming correlagrams up to three off-diagonals of the beam pair matrix [see Fig. 4.1(b)] are used, for a total of 44 beam pair correlations. The beam-cross-beam correlagram appears in Fig. 4.2.

Several details regarding the method used to produce Fig. 4.2 deserve note. The original correlagram consists of 1801 time delay pixels horizontally (6 s x 300 Hz) and 625 recording time pixels vertically. In order to make the image fit on a single page, an interpolation scheme is used to compress the image by a factor of four in the horizontal to a size of 450 by 625. A certain degree of resolution in the traces is lost in the process. Also, the absolute value of the correlagram values is taken before imaging in order to make the traces more distinct. It has been found that with beam-cross-beam correlagrams, the gain in gray-shade dynamic range provided by the unsigned correlagram more than makes up for the lost information. On a

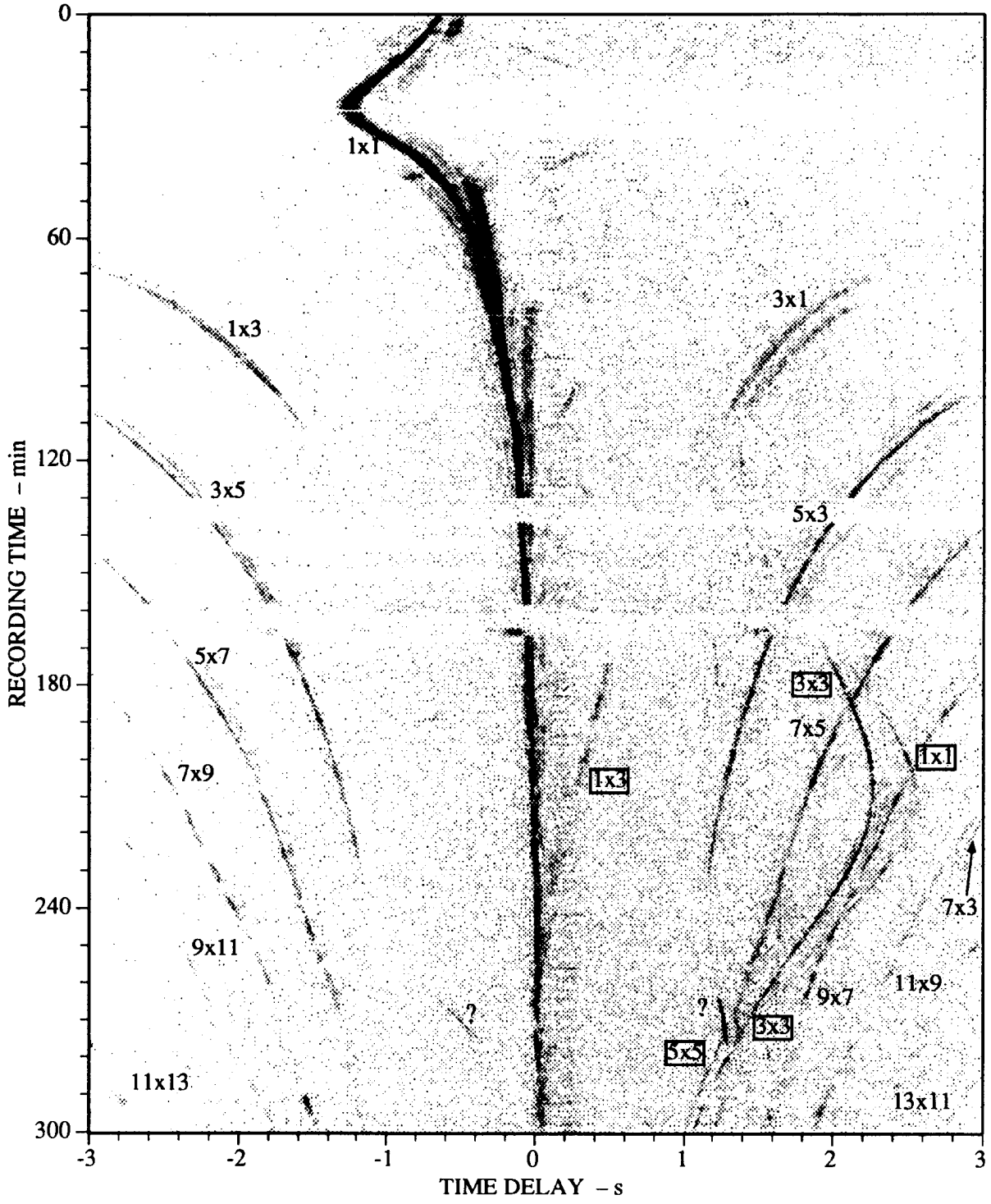

FIGURE 4.2 Beam-cross-beam correlagram for the entire 5 hr time period. The CPAs of the two ships occur at 90 and 205 min. The CPA of ship 1 provides an excellent picture of the multipath correlation structure as a function of range. (AS-94-1061)

signed correlagram the traces tend to contain alternating positive and negative correlations, with the negative ones carrying no additional information.

Finally, in imaging the correlation values, a "μ-law" scheme is used to map correlation value intervals to shades of gray. The scheme uses the following three parameters: $c_{\min}$ and $c_{\max}$, the minimum and maximum correlation values; and μ, the number of levels. Break points c_n are determined by

$$c_n = c_{\min} + \frac{(\mu-1)^{n/(\mu-1)} - 1}{\mu - 2}\left(c_{\max} - c_{\min}\right) \quad , \quad n = 0,1,2, \ \ldots \mu - 1 \quad . \tag{4.2}$$

For the correlagrams shown in this report, μ=16, $c_{\min}$=0.025, and $c_{\max}$=0.25.

In annotating Fig. 4.2, ray paths are specified by the number of ocean traversals (an odd number in the present case of near-surface source and near-bottom receiver) and correlation traces by the ray paths at the two arrays. For example, the 1x3 (pronounced "one-cross-three") trace is produced by the 1-traversal ray (direct path) at array 1 and the 3-traversal ray at array 2. With the help of the simulations to be described shortly, the origin of the traces in Fig. 4.2 have been labeled: those associated with ship 2 have rectangular boxes around them, while those associated with ship 1 do not. The modeled R–θ plot in Fig. 3.3 is also used to find the ranges at which the various eigenray arrivals first become significant and are eventually cut off. Since the beams are steered toward the ocean surface, the positive angles on the R–θ plot are of interest.

4.3 Analysis of Ship 1

The main trace in Fig. 4.2 that bows to the left at 25 min is the 1x1 trace produced by the ship that was used to synchronize the clocks and localize the arrays (see Fig. 2.5). As the ship moves farther out in range, other like-order traces, such as the 3x3, the 5x5, and the 7x7, merge with it and eventually replace it.

The traces in Fig. 4.2 that sweep toward the 1x1 trace from the sides are produced by unlike ray paths. The first traces on the left and right are the 1x3 and 3x1 traces, respectively.* Note that the traces begin around 70 min, when the 3-traversal rays first arrive at grazing angles of 30° or lower, and terminate at 110 min, when the 1-traversal ray path is cut off. From the R–θ plot in Fig. 3.3 the direct-path cutoff occurs at a range of about 33 km, implying

*One can keep track of the order (1x3 versus 3x1) by keeping in mind that the correlator implementation used in this work computes the time delay as the travel time at array 1 minus the travel time at array 2.

that the ship's range at time 110 min is 33 km. If beams at steeper angles are formed, the 1x3 and 3x1 traces should become visible at somewhat earlier times. At very short ranges, however, the 3-traversal rays become weaker due to geometric spreading along their longer path length and reflection loss in the ocean bottom. The weakening of the 3-traversal rays at short ranges can be clearly seen in the R–θ plot of Fig. 3.3.

The next pair of inter-order traces in Fig. 4.2 are the 3x5 and 5x3 traces, which begin just after 100 min, when the 5-traversal ray first arrives at 30°, and end close to 230 min, the time at which the 3-traversal arrival is cut off. According to the R–θ plot in Fig. 3.3, the cutoff of the 3-traversal ray at time 230 min corresponds to a range of 95 km. If the ship is assumed to travel at a constant velocity from CPA at 25 min to a range of 95 km at 230 min, the velocity is 7.7 m/s, which is in good agreement with the estimate of 7.4 m/s made at CPA.

Before the remaining pairs of inter-order correlation traces produced by the ship in Fig. 4.2 are identified, a simulation of the correlagram produced by the broadband ray model (see Refs. 1 and 2) is shown. Figure 4.3 is the result of simulating the broadband fields at the 18 receivers of each array for a ship traveling at 7.42 m/s along the track shown in Fig. 2.4(b). The beam-cross-beam algorithm is applied to the simulated fields in exactly the same manner as it is to the recorded data. Over the 300 min time period simulated, the ship's range to the midpoint of the arrays varies from 11.5 km at 0 min to about 2.7 km at 25 min to 122.5 km at 300 min.

The simulated and measured correlagrams show a strong similarity. The correct modeling of the 1x1 trace near CPA results from the source and array localization done in Sec. 2. The origins of the traces in the correlagram (see labels) are easily identified by examining a list of the eigenrays and their travel times at particular ranges. Careful comparison of Figs. 4.2 and 4.3 reveal that the inter-order traces all the way up to the 9x11 and 11x9 traces can be identified in the measured data. Even the prediction that the 11x9 and 7x3 traces should be side-by-side for a short time period (near 220 min in the data, 240 min in the simulation) appears to be borne out by the data. Good agreement may be observed in the manner in which the 1x3 and 3x1 traces are cut off near time 110 min. A discrepancy of about 20 or 30 min exists in the predicted and measured times of the cutoff of the three-traversal ray. Several explanations are possible: the ship may have increased its velocity, or the bathymetry over the 95 km range over which the ship traveled could have changed.

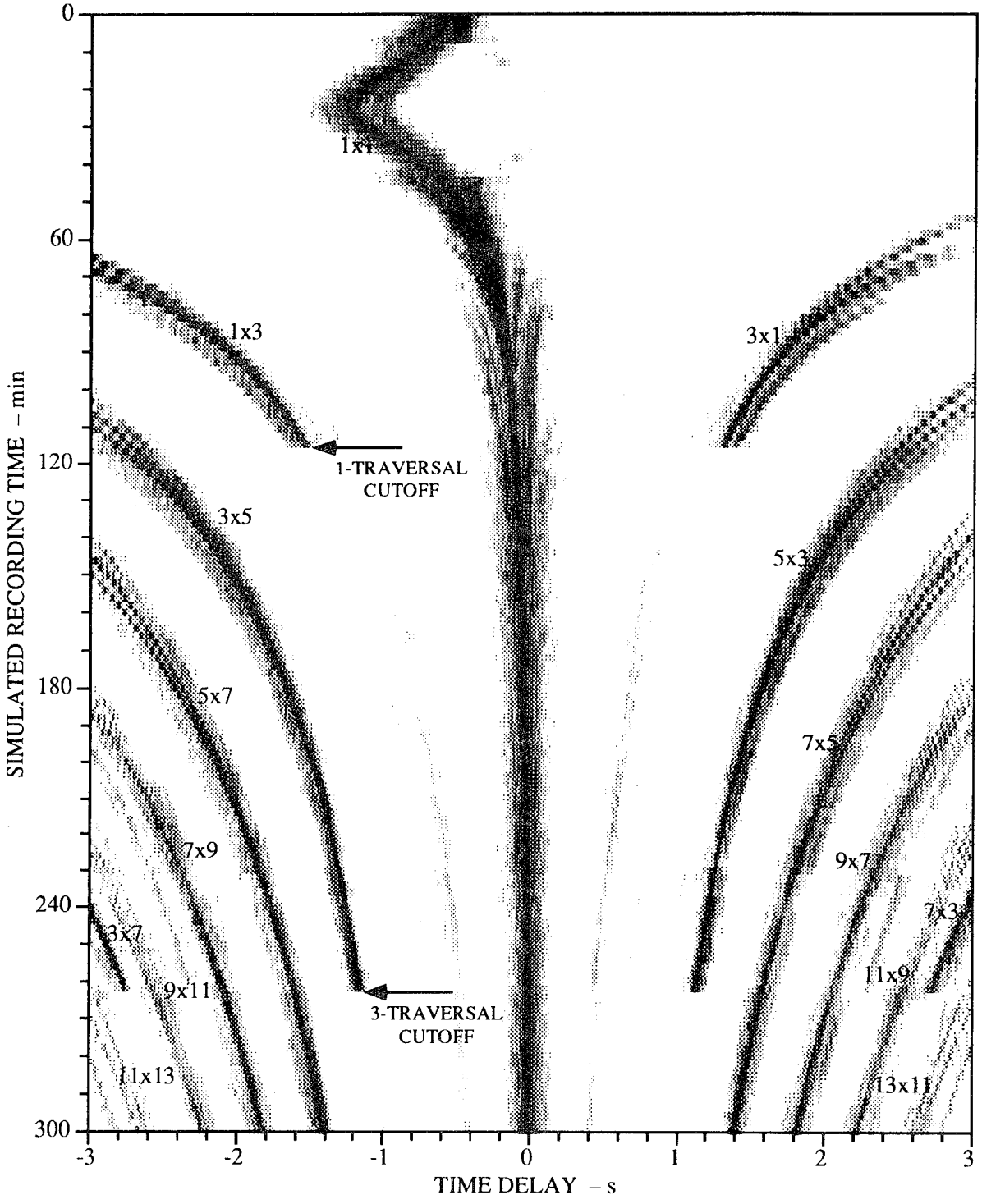

FIGURE 4.3 Simulated correlagram produced by the ship track derived in Sec. 2 [see Fig. 2.4(b)]. (AS-94-1062)

4.4 Localization and Simulation of Ship 2

The CPA of the second ship occurs at time 212 min in Fig. 4.2. As mentioned in Sec. 2, the trace produced by ship 2 is the trace used to determine that the array separation is 3.8 km, rather than 5.3 km. The determination is made by applying a source localization algorithm similar to the one used on the vertical aperture correlations in Sec. 2. As before, the correlation trace is sampled at a number of recording times, and the constant-velocity source track that produces the best fit is found. Since the aperture is horizontal in the present case, the track relative to the array line of bearing, which is assumed to be along the x-axis, is determined.

When applying the source track localization algorithm to the second ship passage, the array separation and the ray paths used to produce the trace are varied because the correct values are not certain. The two possible array separations of 3.8 and 5.3 km and ray paths with 1, 3, and 5 ocean traversals are used. When 1-traversal ray paths are used to simulate the correlagrams, the best-fit correlagram exhibits very poor agreement with the data. When it is assumed that 5-traversal ray paths produce the trace, fair agreement in correlagram traces is obtained only for $d = 3.8$ km, but the derived source velocity is on the order of 15 m/s, which is unreasonably high for a ship. The best fit to the correlagram is obtained assuming 3-traversal ray paths and a separation of $d = 3.8$ km. The best fit correlation trace and the derived source track are shown in Fig. 4.4 and described in detail in the figure caption. When $d = 5.3$ km is assumed, the error in the correlagram fit is four times larger. This analysis provides convincing evidence, from the acoustic data alone, that the array separation is 3.8 km. The estimate of 3.8 km also agrees perfectly with the separation reported at the time of deployment.

A simulated correlagram for the derived source track of ship 2 is shown in Fig. 4.5, where the traces are again labeled according to the ray paths that produce them. Because the simulation is noise-free, many more traces appear in the simulation than appear in the data of Fig. 4.2. The two main traces around CPA, the 3x3 and the 1x1, are well modeled, as is the fainter 5x5 trace. The trace labeled 1x3 in the data was originally thought to be independent of the two ships, but the simulation clearly shows it to be the 1x3 of ship 2. The two traces of short duration (labeled with question marks in Fig. 4.2) around time 270 min in the data appear to be unrelated to the two ships modeled. It is speculated they could have been produced by one of the ships involved in the experiment, which may have turned on its engines for a period of 10 min or so in order to reposition itself.

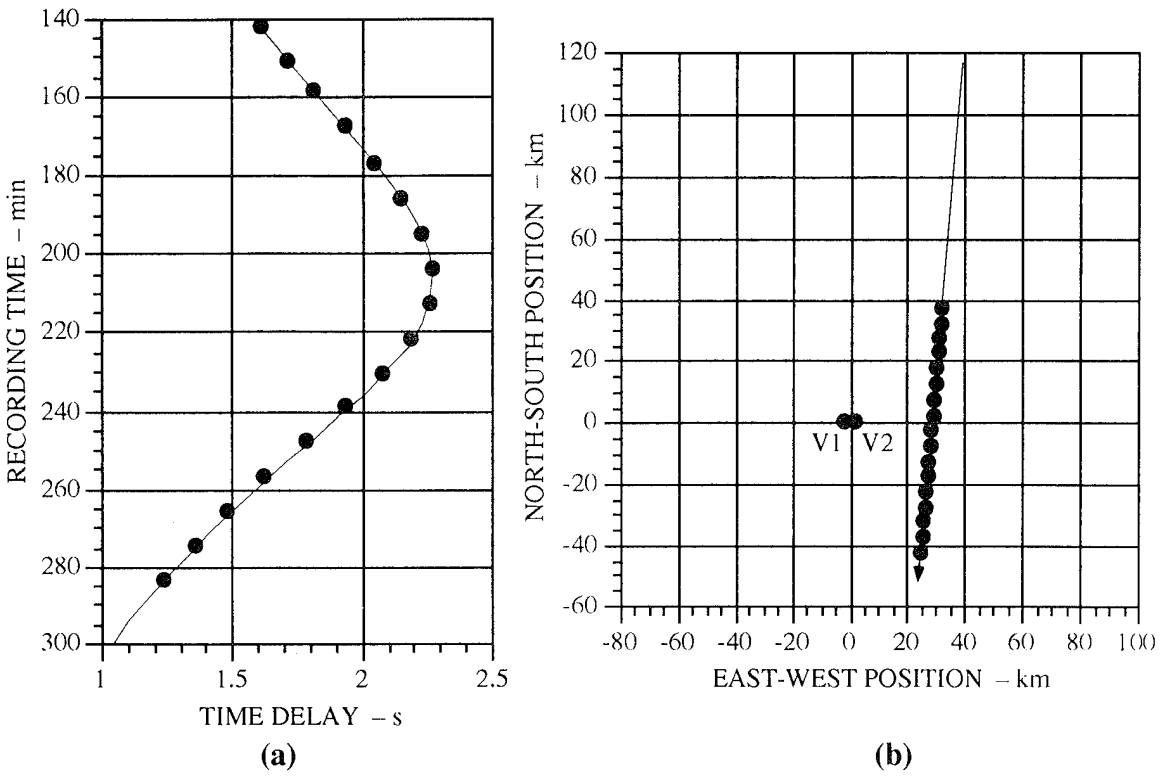

FIGURE 4.4 Source track localization of ship 2: (a) Sampled points from the measured correlation trace (dots) and the derived best fit correlation trace (solid line). (b) Derived source track relative to the two vertical arrays, which lie on the *x*-axis. The dots indicate the locations at the times at which the trace was sampled. The derived ship velocity is 9.4 m/s, the bearing is 185.1°E of N, and the CPA ranges to V1 and V2 are 30.8 and 28.9 km, respectively. (AS-94-1063)

The final modeling exercise is to combine the simulations of ships 1 and 2. The two ships are assigned independent realizations of a white noise source signal, where successive samples of the time-domain signal are independent, Gaussian distributed random numbers. The resulting source spectra are then multiplied by the model-produced transfer functions that account for the propagation to the 36 receivers. The received spectra produced by the two ships are added together, and the beam-cross-beam algorithm carried out as before. Figure 4.6 shows the simulated correlagram for both ships. In order to reproduce the data correlagram of Fig. 4.2 as accurately as possible, ship 1's band-averaged (10–150 Hz) source level is set 18 dB higher than that of ship 2. The agreement between the data and simulation is excellent.

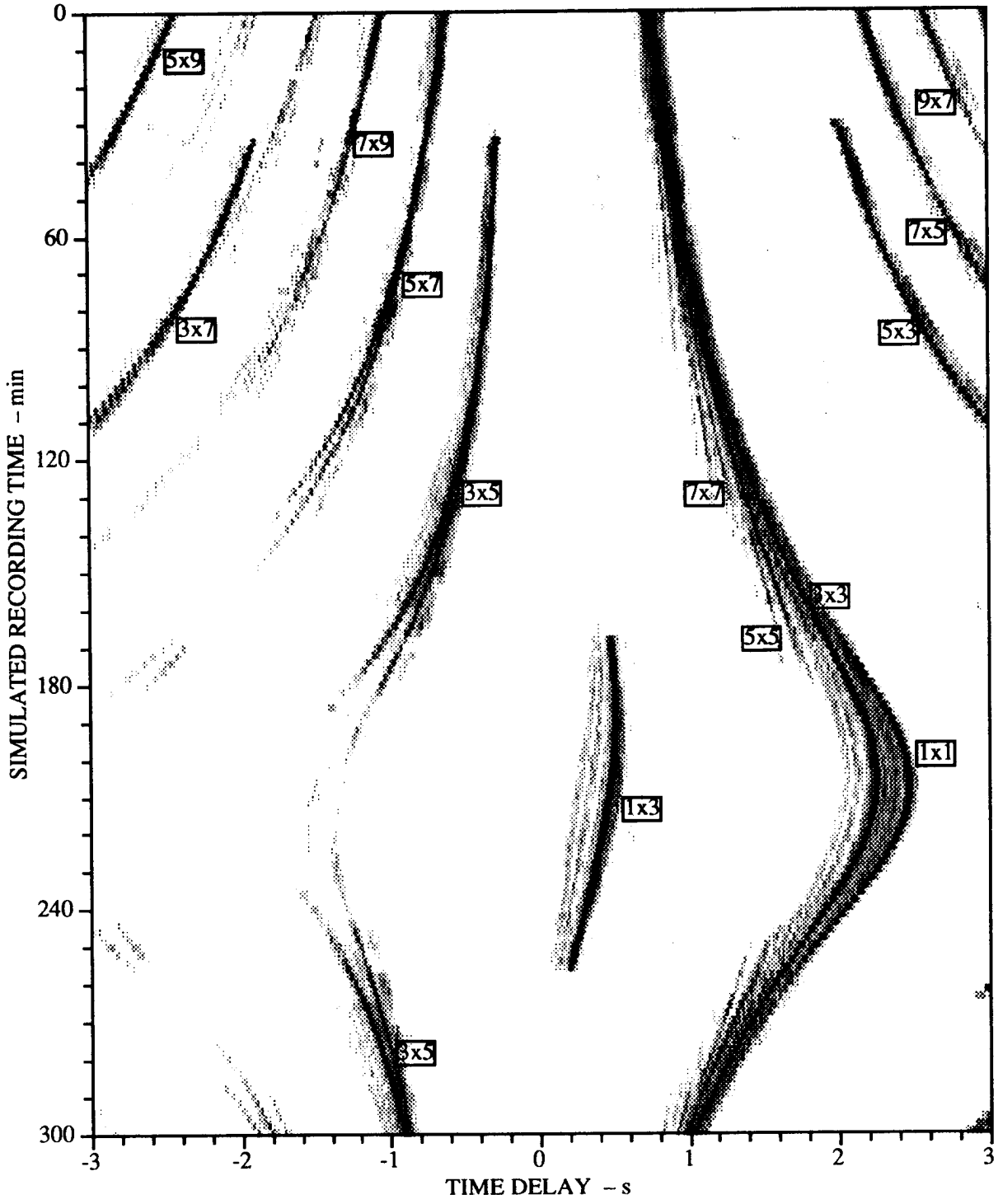

FIGURE 4.5 Simulated correlagram for the derived source track of ship 2. (AS-94-1064)

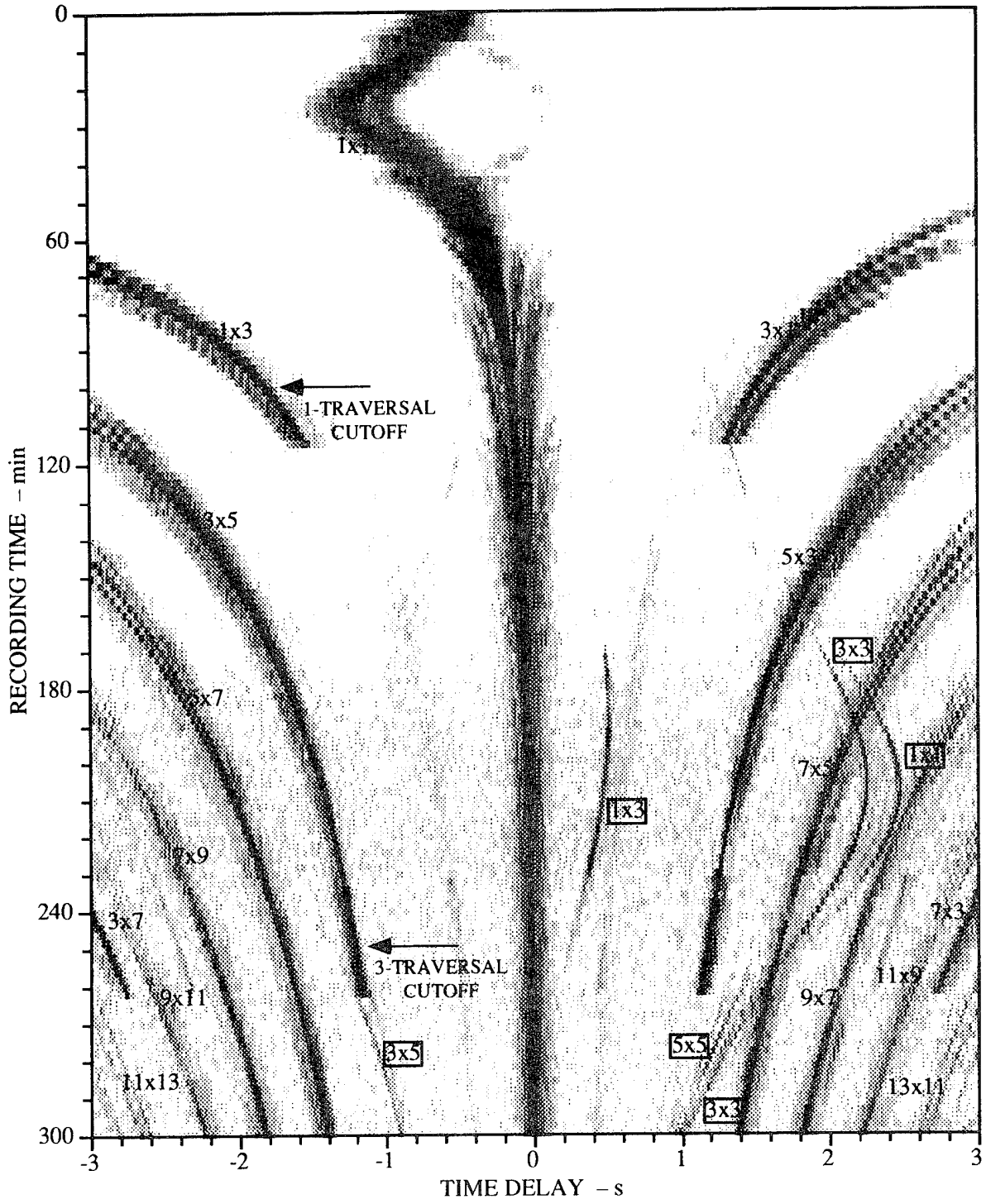

FIGURE 4.6 Simulated correlagram of the superposed signals from ships 1 and 2, to be compared with the measured data in Fig. 4.2. (AS-94-1065)

4.5 Variation of Beam-Cross-Beam Parameters

In this subsection, the manner in which the beam-cross-beam correlagram display varies with certain algorithm parameters is examined. For reference, Fig. 4.7 shows an uninterpolated portion of the beam-cross-beam correlagram that runs from 140–300 min in recording time and from 1–3 s in delay time. Recall that eight beams from 0°–30° are steered, and 44 beam pairs [up to three positions off the main diagonal in Fig. 4.1(b)] are crosscorrelated.

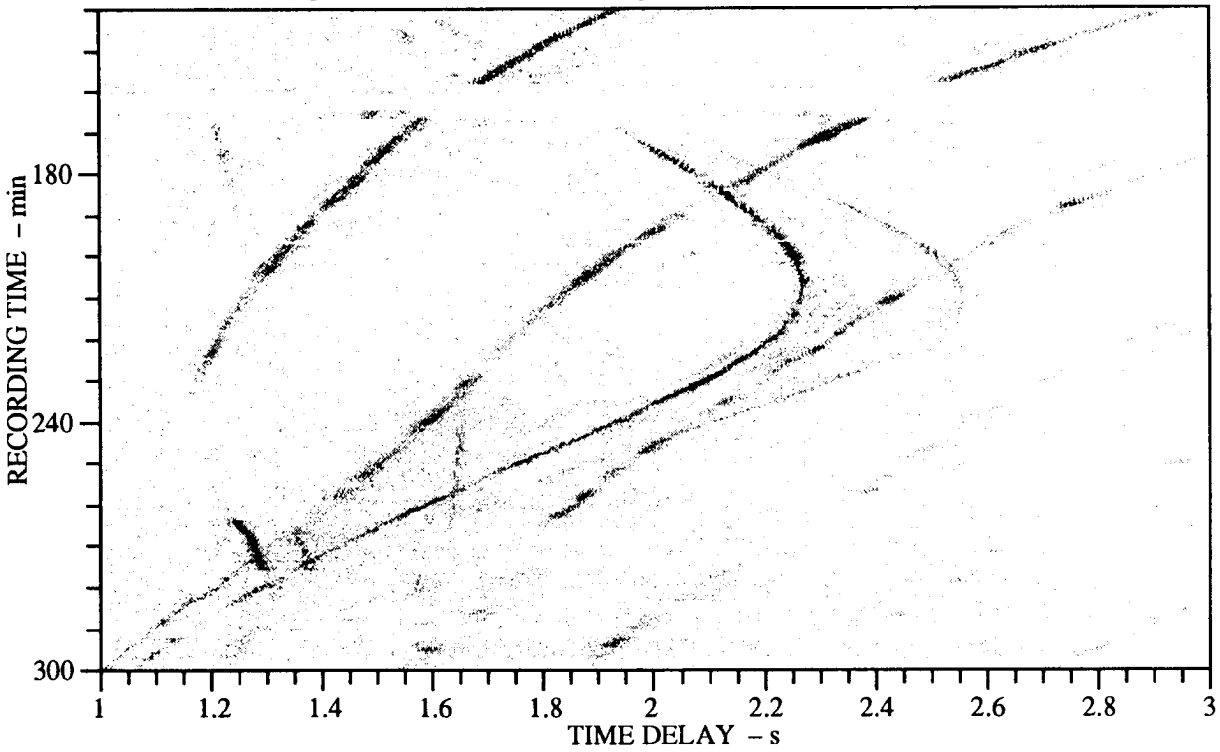

FIGURE 4.7 Uninterpolated portion of the beam-cross-beam correlagram of Fig. 4.2 showing the CPA of ship 2 and the inter-order correlation traces from ship 1. (AS-94-1066)

The effect of performing fewer crosscorrelations is examined first. Figure 4.7 shows the result of using only the main diagonal of the beam pair matrix. Only a very small degradation can be observed in the clarity of the traces, and the noise is actually reduced because fewer correlations are merged. Clearly, the reduction in computing eight instead of 44 correlations is worth the slight degradation in this case. For quiet sources at short range, it is more likely that one may be required to correlate beams steered in different directions, although the fact that the beams at high grazing angles are wider will tend to mitigate that requirement.

The other parameter examined is the range of grazing angles at which beams are steered. Figure 4.9 shows the result of steering 12 beams (equally spaced in sin θ from 16°–90°). The 1x1 trace from ship 2 and the end of the 5x3 trace from ship 1 are missing because at least one

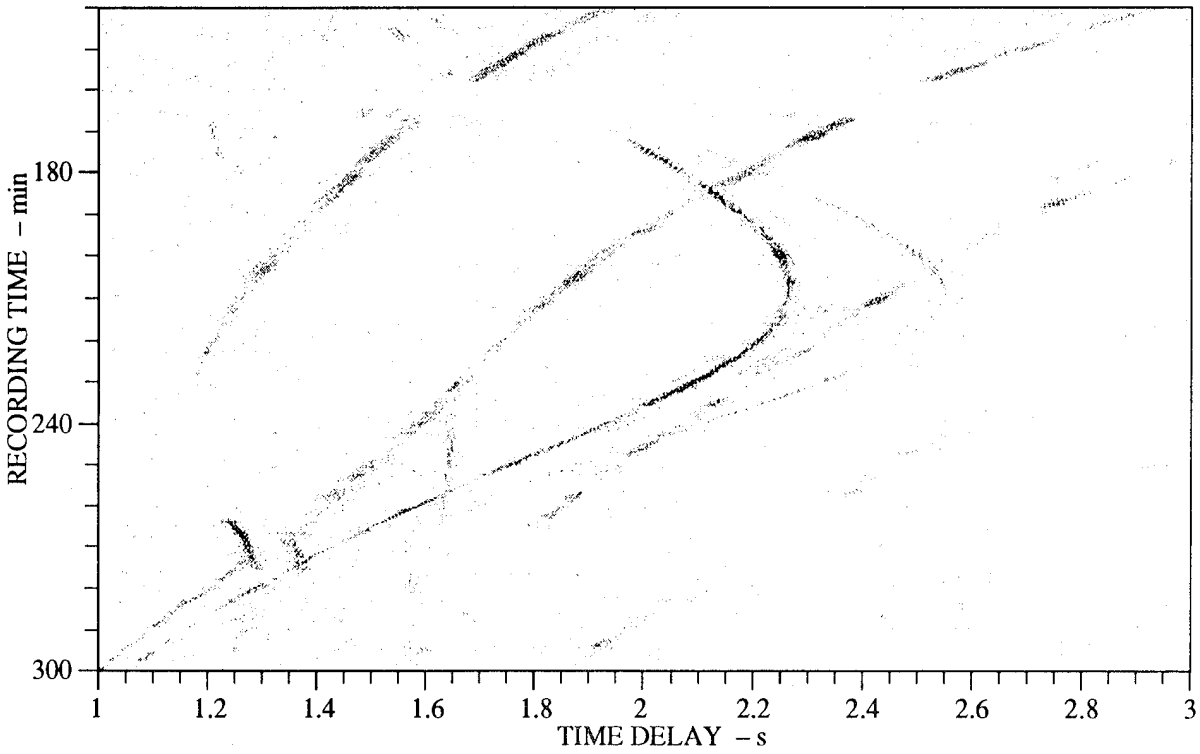

FIGURE 4.8 Beam-cross-beam correlagram formed by crosscorrelating only beams steered at the same angle (the diagonal of the beam pair matrix). (AS-94-1066)

of the rays involved in each correlation arrives at angles shallower than 16°. The two short traces at times 180 and 250 min, which have not been associated with either ship, are also missing. The slight reduction in noise that is evident in Fig. 4.9 compared to Fig. 4.7 is probably due to the fact that fewer beams at the noisy low angles are used. By steering at the steeper angles it was hoped to detect any quiet, short range noise sources that may have been present, but the lack of any additional traces suggests that none were present.

4.6 Sector-Focused Beam Patterns

As stated at the beginning of this section, an important issue that needs to be addressed when considering the beam-cross-beam correlation algorithm is that of choosing the number of beams to steer and the number of beam pairs to crosscorrelate. One way to reduce the number of correlations required is to use sector-focused beam patterns instead of the usual "pencil beams" that result from CBF and ABF. The array pattern of a sector beam exhibits a broad plateau over a desired range of steering angles. The beneficial qualities of a pencil beam sacrificed by forming a broad plateau are increases in the peaks of the sidelobes outside the region of interest and rippling in the passband.

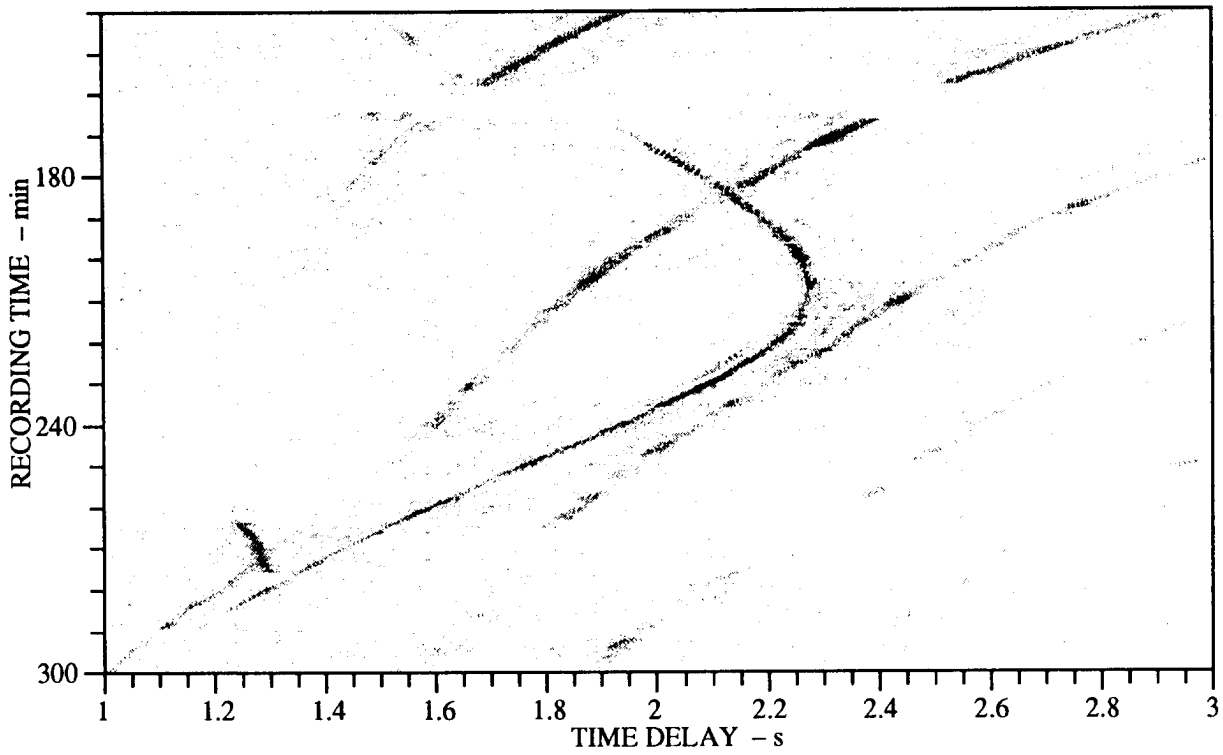

FIGURE 4.9 Beam-cross-beam correlagram formed by steering beams from 16°–90°. (AS-94-1067)

A technique developed by Stutzman and Coffey,[4] called the iterative sampling method (ISM), is used to synthesize the desired beam patterns. One of the advantages of the method is that the desired beam pattern is specified by intervals of acceptable response levels for given intervals of steering angles. Transition intervals between passbands and stopbands also need to be specified. Most other methods require the specification of a discrete number of points in the beam pattern, and the synthesized beam pattern can behave erratically between those points. The ISM algorithm consists of making an initial guess at the steering weights, computing the beam pattern, finding the angle at which the beam pattern most violates the desired specification, and then "fixing" the beam pattern in the "bad" direction. The beam pattern is fixed by steering a uniformly weighted beam in the bad direction and assigning the weights a factor that assures the sum of the old beam pattern and the uniformly weighted beam pattern has the desired response in the bad direction. The cycle of computing the beam pattern and fixing it continues until the specification is met or a given limit on the number of cycles is reached. Since the processing is broadband, the ISM algorithm is applied at frequency intervals of 5 Hz, and the weights are interpolated as required.

In order to compare the sector beam results to the pencil beam results of Fig. 4.2, a sector beam pattern that has a passband from 0°–30° is specified. The stopband levels are desired to be at least 20 dB down, the ripple in the passband is desired to be within ±2 dB of zero, and transition intervals of 6° are allowed about the transition points of 0° and 30°. The synthesized beam pattern as a function of frequency (from 15–140 Hz) and steering angle for array V2 is shown in Fig. 4.10. It is evident that at the low and high ends of the frequency band the desired beam pattern could not be obtained, and that the best beam patterns occur around a frequency of 80 Hz. The broadband beam pattern synthesis for V1 was somewhat less successful, in part because the array is uniformly spaced.

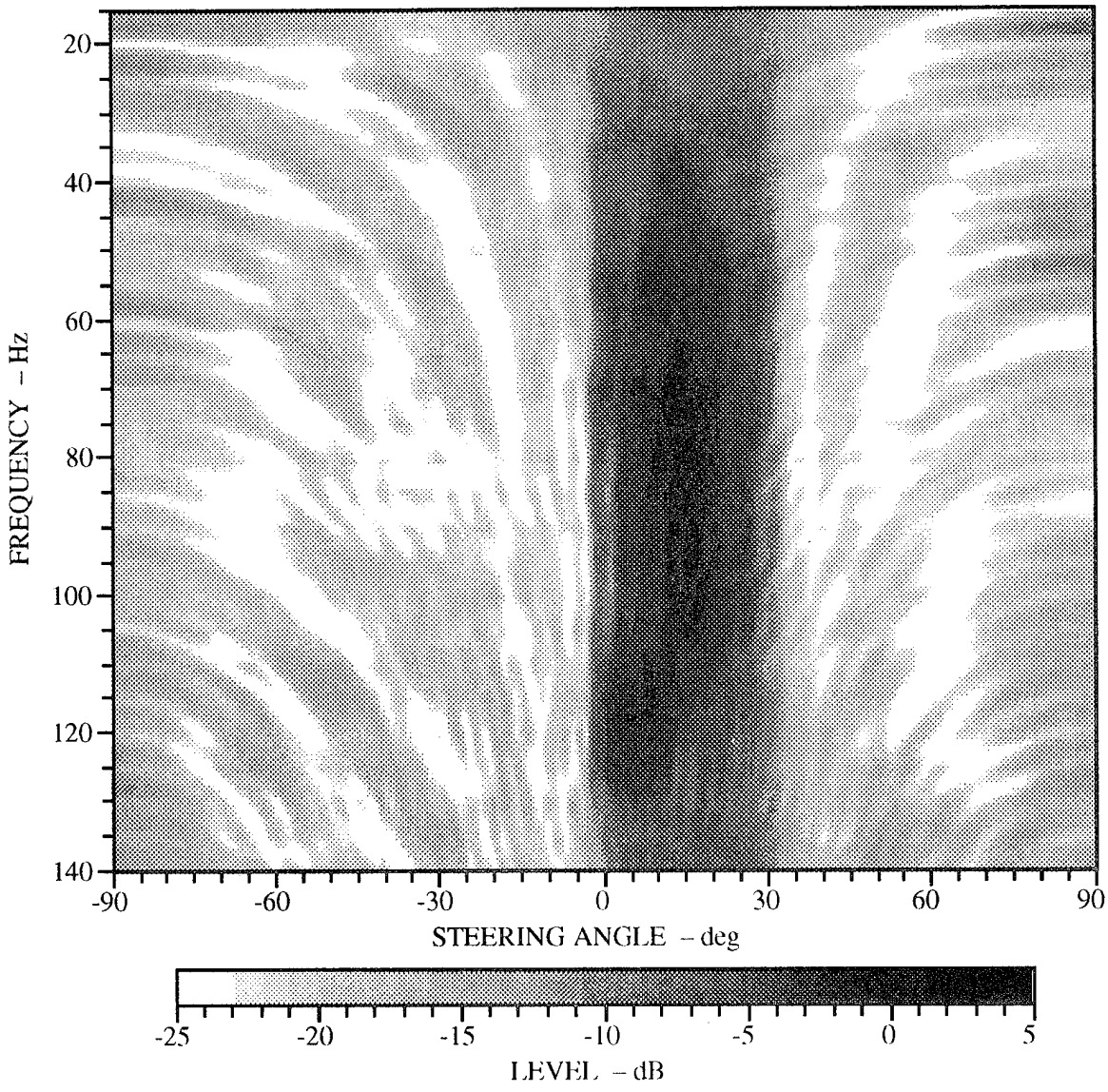

FIGURE 4.10 Broadband beam pattern synthesized using the ISM algorithm for V2 for a passband of 0°–30°. (AS-94-1068)

When sector beam patterns are used on both V1 and V2 so that only one beam is formed at each array and only one correlation is required, the result is quite poor and is not shown here. A somewhat more expensive alternative is to use eight pencil beams on V1 and a sector beam on V2, which requires just eight correlations to be performed and merged. The correlagram that results is shown in Fig. 4.11. Compared to the reference correlagram of Fig. 4.2, the higher order traces produced by ship 1 and some of the traces produced by ship 2 do not appear as strongly in Fig. 4.11. For this particular application, it appears that the pencil-cross-sector correlagram is also inferior to the pencil-cross-pencil correlagram in Fig. 4.7, which uses only the eight correlations along the main diagonal of the beam pair matrix. In other applications, where the arrays are specifically designed to provide good broadband beam patterns, the sector pattern approach may be worth investigating, but in the present case it is not worthwhile.

A potential problem with the sector beam approach is that a signal arriving at the two arrays may be distorted by the beamformer so that the coherence between the two beamformer outputs is reduced. The complex beamformer response as a function of frequency may be viewed as a transfer function that may distort an impulsive signal arriving at the array. Pencil beams, such as the Taylor shaded beams used in this work, are non-distorting because they have unity gain and zero phase in the look direction at all frequencies. Sector beams, on the other hand, do not set any requirements on the phase of the response. If the phase of the beamformer transfer function is not linear with frequency, the impulse response is distorted, and if the two beamformers distort the impulse in different ways, the values obtained by correlating the beamformer outputs are reduced. Examination of the phase of the beamformer response for the synthesized patterns shown in Fig. 4.10 indicates that the phase is fairly linear as a function of frequency, but does exhibit some ripples. Additional work with sector beams should include an analysis of the distortion effects. The possibility of optimizing the array geometry for sector beamforming should also be investigated.

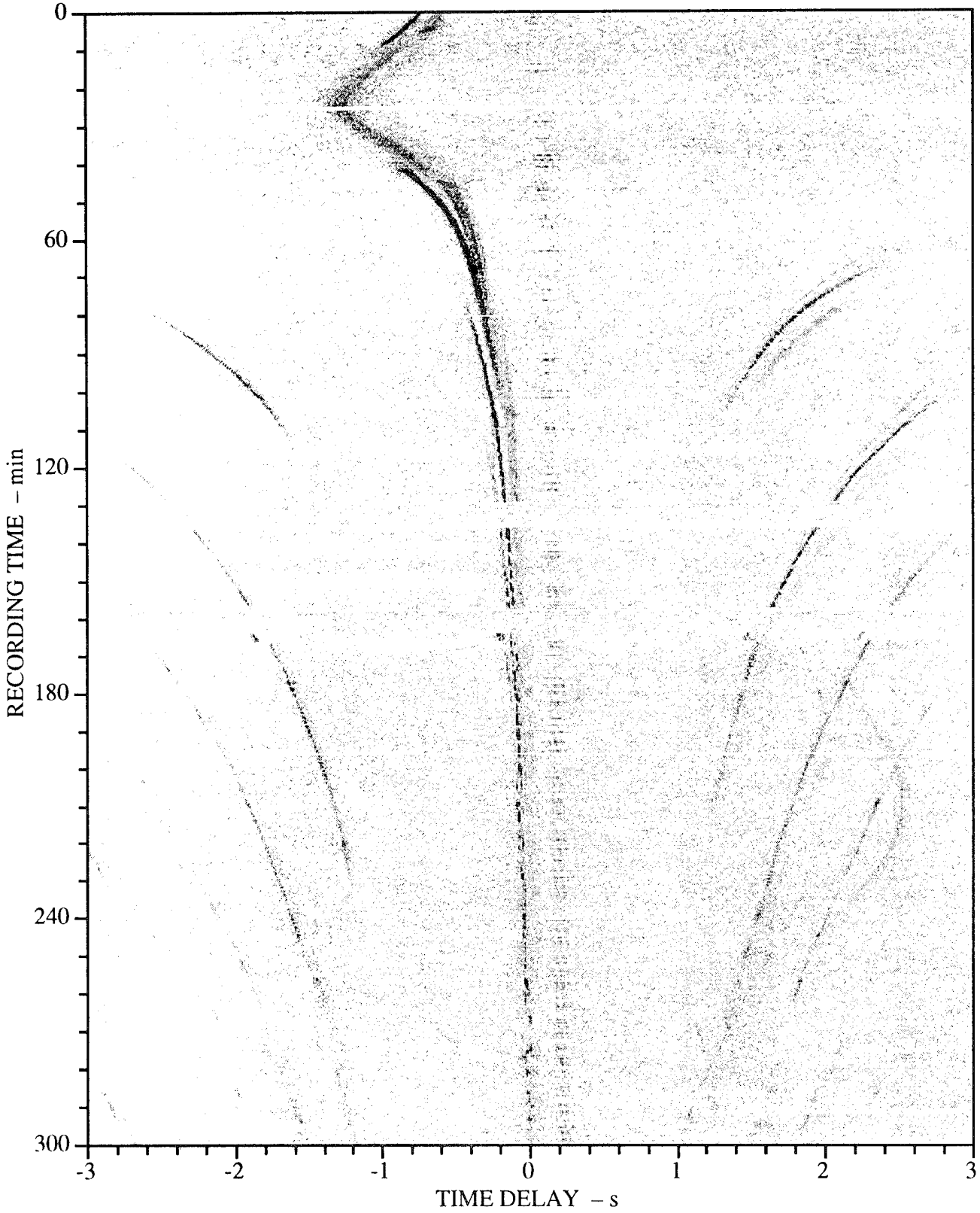

FIGURE 4.11 Beam-cross-beam correlagram produced by steering eight pencil beams at V1 and one sector beam at V2. (AS-94-1069)

This page intentionally left blank.

5. SIMULATED DETECTABILITY OF QUIET SOURCES

In forming the beam-cross-beam correlagrams in the previous section, beams were formed at shallow grazing angles (0°–30°) in order to focus on the passing ship traffic. In anti-submarine warfare (ASW) applications, the objective more often is to search for quiet sources at relatively short ranges. Beams are steered at steeper angles, say from 30°–90°, in order to discriminate against the horizontally arriving distant shipping noise. In this section the beam-cross-beam algorithm for ASW applications is evaluated by "injecting" a simulated source field into the recorded data. The detectability of various sources of interest, as a function of source level and detection range, can thus be investigated using real-world background noise measurements.

The simulation procedure consists of the following steps:

1. Propagation from a source to the elements of the two arrays is simulated using the broadband ray model. The complex field versus frequency at each receiver is called the transfer function.
2. The simulated source spectrum $S(f)$ is generated by first taking the discrete Fourier transform of a time series $s(t)$ whose samples are independent realizations of Gaussian distributed noise. The spectrum is then given a realistic shape by multiplying by a frequency filter that rolls off 6 dB/octave from 10 Hz to 150 Hz. Finally, the broadband (10–150 Hz) source level *SL* of the spectrum is adjusted so that

$$SL = 10\log\left[\frac{1}{N\Delta f}\sum_{f}|S(f)|^2\right] \quad . \tag{5.1}$$

3. The field at the arrays is simulated by multiplying the transfer functions by the source spectrum.
4. The simulated data at each receiver are added to the measured data.
5. The data are processed according to the beam-cross-beam algorithm.

6. The detectability of the source is evaluated by searching for traces corresponding to the quiet source in the beam-cross-beam correlagram.

5.1 Stationary Source with Increasing Level

For the first simulation a source is placed at a particular location, and its level is allowed to rise as a function of time. The source-receiver geometry is illustrated in Fig. 5.1. The source is at depth 100 m and is 3.6 km from the midpoint of the two arrays, at a bearing of 60° from broadside. The ranges to V1 and V2 are 5.3 and 2.2 km, respectively, and the grazing angles of the direct path eigenrays are 38.2° and 63.1° respectively. The simulated source field is added to the measured data from minutes 160–300, during which time the 10–150 Hz band-averaged source level increases linearly from 110 dB to 140 dB. The source-injected data at each array are then beamformed at the steering angle corresponding to the direct path eigenray,* and the beamformer outputs are crosscorrelated.

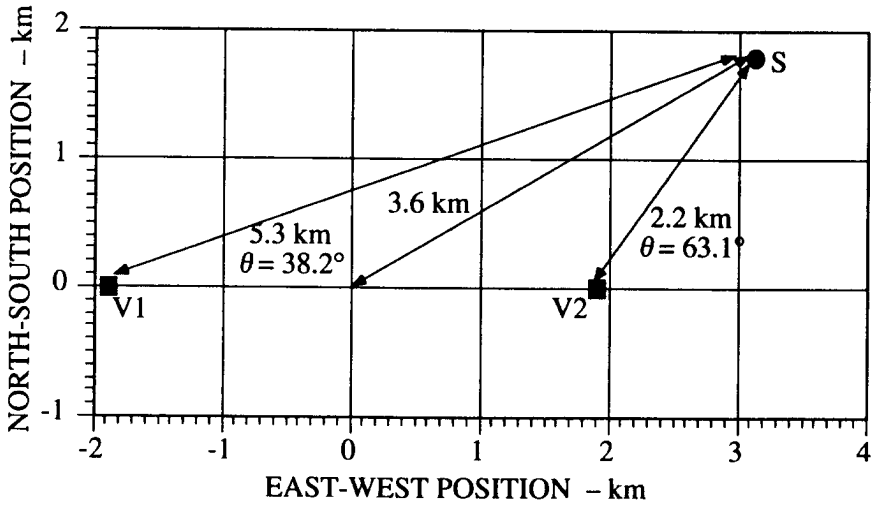

FIGURE 5.1 Source-receiver geometry for the stationary source with increasing level. (AS-94-1070)

The beam-cross-beam correlagrams for the stationary source case using ABF and CBF are shown in Fig. 5.2. The left-hand axis in the figures indicates the recording time, while the right-hand axis indicates the band-averaged source level. The four traces that emerge from the background noise are labeled according to the ray paths (D for direct, S for surface-reflected) that produce them. From the points where the traces first become visible, the minimum detect-

*A priori knowledge of the arrival angles is assumed in order to illustrate the best possible detection scenario. In the real world, multiple beams would be steered, and multiple correlations performed.

able levels using ABF and CBF are about 121 dB and 129 dB, respectively. Note how "quiet" the correlagram appears, despite the presence of the two loud ships in the vicinity.

The price of ABF's 8 dB advantage over CBF is increased processing time. In order to perform broadband ABF, one must form cross-spectral matrices (CSMs), compute ABF weights, and apply those weights to the original spectra from which the CSMs were formed. In forming CSMs, 131 center frequencies in the 10–140 Hz band are used. Frequency averaging is over 1-Hz bands (14 FFT bins), and time averaging is over two recording time intervals. ABF weights are computed at 131 center frequencies. When applying the ABF weights back to the FFTs, the weights for each receiver are linearly interpolated across the 1-Hz intervals between center frequencies. In contrast, broadband CBF is implemented by beamforming the FFTs directly with Taylor-shaded weights. On ARL:UT's Alliant FX8 computer, the ABF procedure requires a total of about 130 min of CPU time, while the CBF computations require just 12 min.

A final point regarding the beam-cross-beam correlagram concerns the fact that the DxD and SxS correlation traces do not coincide. The reason, of course, is that the ranges from the source to the two arrays and the ray arrival angles at the two arrays are quite different, which in turn is because the separation between the two arrays is not small compared to the ranges. When the DxD and SxS correlation traces do not coincide, the signal arriving along the surface-reflected ray path, although coherent with that arriving along the direct path ray, behaves as noise in relation to it. If the signals on the two ray paths are of equal magnitude and the DxD and SxS traces do not coincide, the highest correlation value possible is 0.5, a loss of 3 dB compared to the value of 1.0 when they do coincide. Regardless of the relationship between the ranges and the array separation, the DxD and SxS traces *do* coincide when the source is broadside to the two arrays. The potential loss of 3 dB in correlation peak may be an important factor in the design of twin VLA configurations.

5.2 Moving Source at Constant Level

For the second scenario, the passage of a 125 dB source at a depth of 100 m along the track illustrated in Fig. 5.3 is simulated. The source travels at a speed of 2.5 m/s and covers 10.5 km in the 70 min time period simulated. The simulated data are added to the experimentally measured data from times 230–300 min, as labeled in the figure. The CPA range to the midpoint of the arrays is 1.8 km.

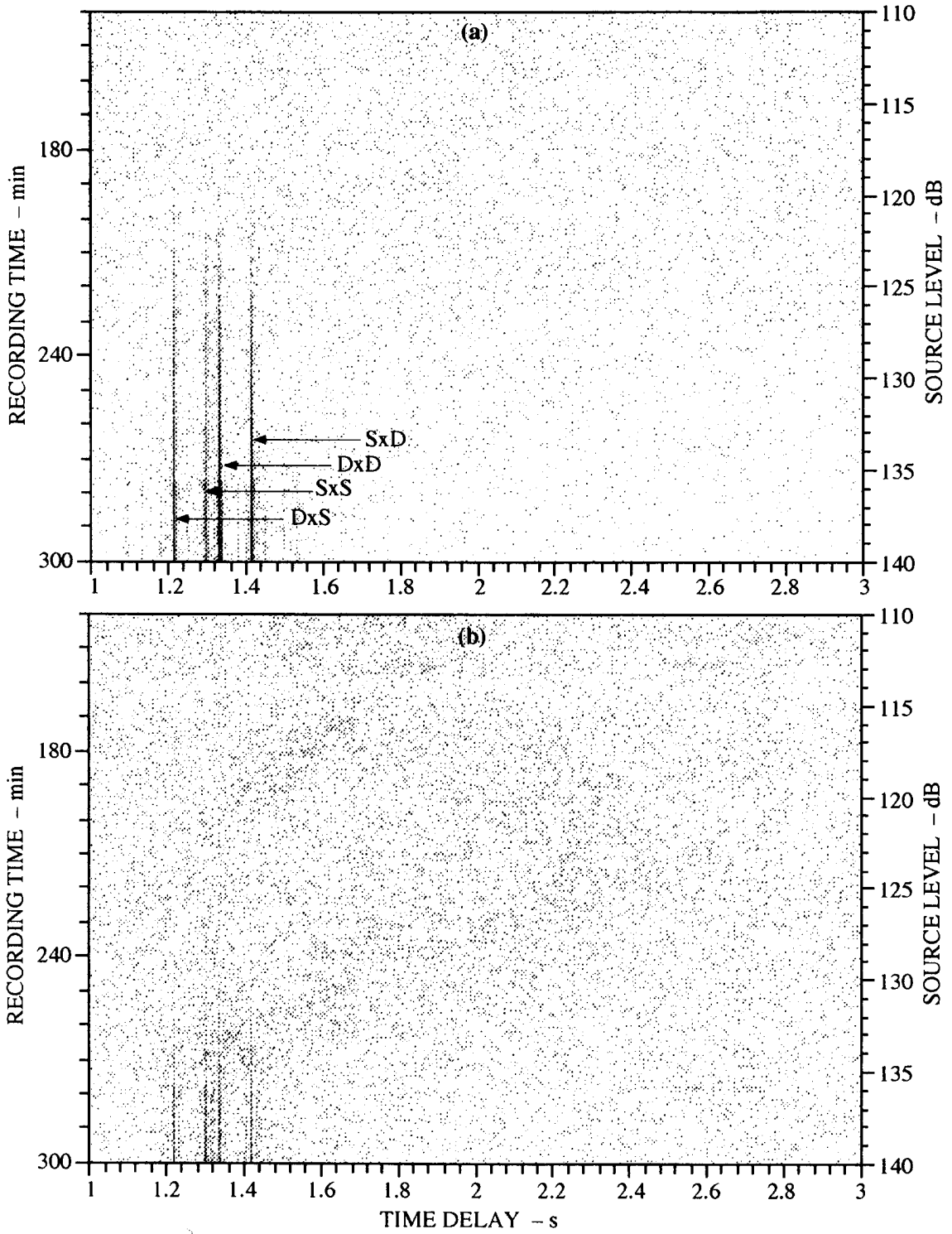

FIGURE 5.2 Beam-cross-beam correlagrams using (a) ABF and (b) CBF for a simulated source at 3.6 km. The band-averaged level of the source as a function of time is shown in the right-hand axes. The minimum detectable levels are about 121 dB and 129 dB for ABF and CBF, respectively. (AS-94-1071)

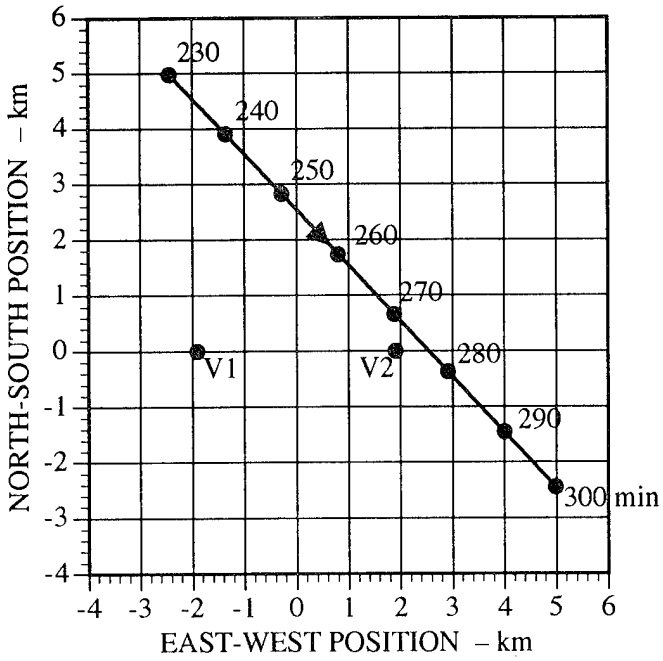

FIGURE 5.3 Source-receiver geometry for the constant-level source moving at a speed of 2.5 m/s. (AS-94-1072)

Unlike the previous case, where the source is stationary, beams must be steered at multiple angles in order to track the moving source. Eight ABF beams are steered evenly spaced in sin θ, from 30°–90°, and beam pairs that are up to four entries off the main diagonal of the beam pair matrix (see Sec. 4.1) are crosscorrelated. The resulting beam-cross-beam correlagram is shown in Fig. 5.4. Detection of the source is possible from time 250 min onward, although it is tenuous during the final 15 min of the time period. Note that the correlation trace becomes the most clear when the source is broadside to the two arrays (around time 253 min), even though the CPA occurs a short time later around 265 min. As discussed in the previous subsection, the enhancement of the trace at broadside occurs because the DxD and SxS traces coincide. When CBF is used instead of ABF, no detection of the source is possible. Also, when the source level is reduced to 120 dB, even ABF beams are not able to detect the source.

It should also be noted that the simulation procedure does not attempt to account for the differential Doppler effects that can decorrelate signals arriving at horizontally separated arrays. For the case in hand, where the array separation is not small compared to the detection range, the potential for Doppler-induced decorrelation is high because a source at short range is likely to be approaching one array while going away from the other. The design of 2-VLA sensors must include such considerations.

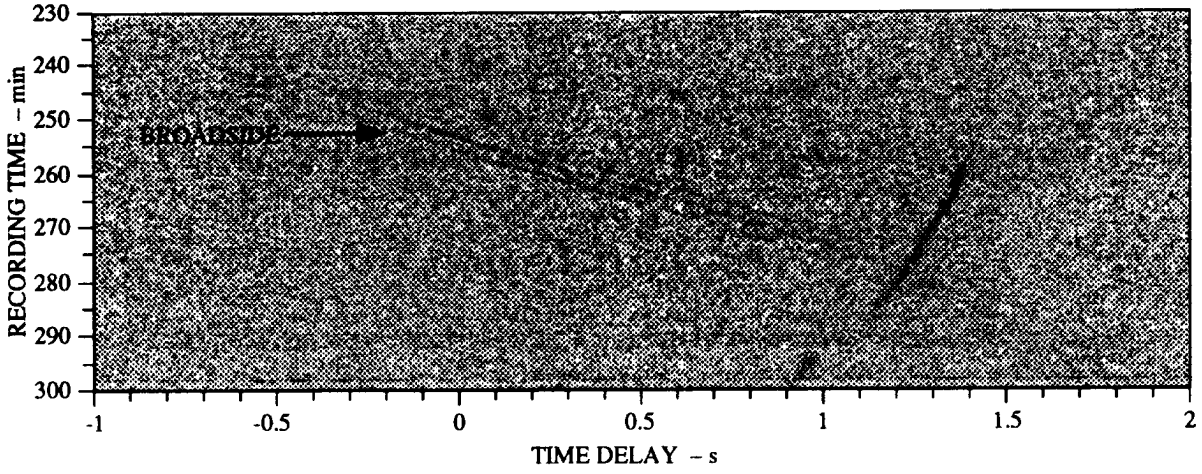

FIGURE 5.4 Beam-cross-beam correlagram for the 125 dB source moving along the track shown in Fig. 5.3. (AS-94-1072)

5.3 Sonar Equation Analysis of Simulated Detections

In this section the simulated detection results are analyzed in terms of the sonar equation. For the crosscorrelation of beamformer outputs, the sonar equation may be written

$$SE = SL - TL - BN - RD \ , \tag{5.2}$$

where *SE* is the signal excess, a measure of detectability; *SL* is the band-averaged source level; *TL* is the transmission loss; *RD* is the recognition differential, a measure of the gain achieved by the broadband crosscorrelation procedure; and *BN* is the beam noise measured in the absence of the source signal in the direction in which the crosscorrelated beams are steered. *SE* is set to zero in order to find the onset of detectability.

For the stationary source case considered in Sec. 5.1, the values for the sonar equation parameters are given in Table 5.1. $SL_{\min}$ is the minimum source level that is detectable and is taken from the simulated correlagrams of Fig. 5.2. Transmission loss is that of the direct path eigenray as computed by the ray model. Band-averaged beam noise values are taken from measured beamgrams. The *TL* and *BN* values at V1 and V2 are combined by taking the geometric mean in linear units, which corresponds to the arithmetic mean in decibels. Finally, the values for *RD* are computed from the sonar equation with *SE* set to zero. The values of -16.5 and -17.1 for RD from Table 5.1 are consistent with the nominal value of -15 dB that has been derived from experience with broadband crosscorrelation.

TABLE 5.1 Sonar equation parameters for the stationary source case.

	ABF			CBF		
	V1	V2	Mean	V1	V2	Mean
$SL_{\min}$	—	—	121.0	—	—	129.0
TL	76.5	73.6	75.1	76.5	73.6	75.1
BN	61.8	63.0	62.4	70.9	71.1	71.0
RD	—	—	-16.5	—	—	-17.1

This page intentionally left blank.

6. SUMMARY AND CONCLUSIONS

In this report a method has been introduced for broadband detection of acoustic sources using two horizontally separated vertical line arrays and the method applied to measured data from the TAGEX 87 experiment. The detection algorithm, which is referred to as "beam-cross-beam correlation," consists of beamforming the two vertical arrays, crosscorrelating selected pairs of beams, and combining the multiple correlagrams into a single display image. When the method is applied to a given ocean environment, array geometry, and source threat scenario, the issues that need to be addressed include the following: (1) the direction and number of vertical beams that are to be steered, (2) the method for choosing the beam pairs to be crosscorrelated, and (3) the method for merging the correlagrams into one display.

Before the beam-cross-beam correlation method could be applied to the TAGEX 87 data set, the two independent clocks of the vertical arrays had to be synchronized, and the separation between the arrays had to be determined. Both tasks were accomplished using the received signals from a loud ship that passed near the arrays.

A 5 hr time period of the data set, which included the loud ship passage, was analyzed in detail. Beamforming of the two vertical arrays separately resulted in noise directionality plots that contain two main features: (1) the multipath arrival structure of the loud ship as it moved out in range, and (2) a broad, flat noise plateau centered about zero grazing angle, which is produced by distant shipping. The multipath arrival structure of the ship agreed well with ray model predictions for the eigenray arrival structure from a surface source moving out to ranges on the order of 120 km. Traces on the noise directionality plots produced by eigenrays with up to nine ocean traversals (four to five bottom interactions) were observed.

The results of applying the beam-cross-beam method to the TAGEX 87 data set were quite interesting. Since no short-range, quiet sources were present during the 5 hr time period studied, beams were steered at shallow vertical angles (eight beams from 0°–30°) in order to enhance detection of the medium- to long-range ships. The beam-cross-beam correlagram exhibited distinct correlation traces produced by two surface ships: the nearby ship used for clock synchronization and a more distant ship that CPAed at a range of about 29 km. Simu-

lated beam-cross-beam correlagrams produced by the two ships, individually and combined, exhibited remarkably good agreement with the measured data. The effects of varying algorithm parameters, such as the number of beam pairs correlated and the range of beam angles steered, were studied. The idea of using sector-focused beam patterns, instead of the traditional pencil beams, was investigated as well.

The second ship that CPAed the arrays was localized using a method that finds the straight-line, constant-velocity source track that produces a best fit to the measured correlation trace. The method uses a table of travel time versus range produced by a ray model to simulate the correlation traces produced by particular eigenray paths. The trace used for localization of the second ship was produced by eigenrays that traversed the ocean three times. The trace fitting technique is a promising method for localizing sources in conjunction with sensors that employ broadband crosscorrelation across a horizontal aperture.

The final study described in this report involved injecting simulated signals from quiet submarine-like sources into the measured data in order to examine the beam-cross-beam algorithm's ability to detect quiet sources in realistic noise environments. In the first case, a stationary source at 3.6 km, projecting broadband energy at increasing levels as a function of time, was injected into the measured data. Beams were steered directly at the source. The time of onset of the trace in the beam-cross-beam correlagram indicated the minimum detectable source level. It was found that beamforming using ABF resulted in initial detection at a source level of 121 dB, which is about 8 dB lower than when using CBF. In the second case, the injected signals were from a 125 dB source transiting the area, and eight ABF beams were formed from 30°–90° at each array. The source was detected at ranges up to about 5 km. A source 5 dB quieter was not detected at all, however.

In conclusion, the author wishes to emphasize three main points regarding the beam-cross-beam algorithm as applied to the TAGEX 87 data set. First, propagation characteristics in the deep water, basically range-invariant environment of the TAGEX 87 experiment are well understood and well modeled. The vertical noise directionality structure consists of a discrete, relatively high angle component due to short- and medium-range shipping and a continuous, low-angle component due to long-range shipping. Second, the beam-cross-beam algorithm for the 2-VLA sensor configuration is effective in detecting quiet sources at short ranges. Finally, injecting signals from simulated submarine-like sources into measured data is a very useful and powerful tool for evaluating exising sensor configurations and designing new ones.

REFERENCES

1. E. K. Westwood and P. J. Vidmar, "Eigenray finding and time series simulation in a layered-bottom ocean," J. Acoust. Soc. Am. **81**, 912-924 (1987).

2. E. K. Westwood and C. T. Tindle, "Shallow water time series simulation using ray theory," J. Acoust. Soc. Am. **81**, 1752-1761 (1987).

3. H. Cox, R. Zeskind, and M. Owen, "Robust Adaptive Beamforming," IEEE Transactions on Acoustics and Signal Processing **ASSP-35**, 1365–1376 (1987).

4. W. L. Stutzman and E. L. Coffey, "Radiation Pattern Synthesis of Planar Antennas Using the Iterative Sampling Method," IEEE Trans Antennas Propagat. **AP-23**, 764–769 (1975).

This page intentionally left blank.

17 October 1994

DISTRIBUTION LIST FOR
ARL-TR-94-18
Technical Report under Contract N00039-91-C-0082
TD No. 01A1030, Spatial and Temporal Signal and Noise Analysis

Copy No.

Commanding Officer
Naval Command, Control, and Ocean Surveillance Center
RDT&E Division
San Diego, CA 92152-5000

1 Attn: D. Barbour (712)
2 H. Bucker (30)
3 C. Persons (732)
4 J. Price (7105)
5 J. Ehlers (7105)
6 N. Booth (541)
7 A. D'Amico (734)
8 D. Hanna (702)
9 J. Lockwood (734)
10 M. Morrison (705)

Commander
Space and Naval Warfare Systems Command
2451 Crystal Drive
Arlington, VA 22245-5200

11 Attn: CAPT W. Hatcher (PMW182-1)
12 J. Feuillet (PMW182-42)
13 CAPT G. Whiting (PMW182)
14 R. Snuggs (PMW182T)
15 CDR D. Liechty (PMW182OC1)
16 T. Higbee (PMW182-1A)
17 LCDR M. Chipkevich (PMW182-141)
18 J. Thornton (PMW182-1)
19 R. Cockerill (PMW182-15)
20 G. Gotthardt (PMW182-21)
21 L. Fabian (PMW182-3)
22 R. Hobart (PMW184)
23 CAPT R. Goldsby (PMW184A)
24 LCDR J. Flayharty (PMW184D)

Office of Naval Research Field Detachment
1020 Balch Blvd.
Stennis Space Center, MS 39529-7050

25 Attn: E. Chaika (Code 124A)
26 B. Adams (Code 110A)
27 J. Matthews (Code 222)
28 H. Ali (Code 245)

Distribution List for ARL-TR-94-18 under Contract N00039-91-C-0082,
TD No. 01A1030
(cont'd)

Copy No.

Office of the Chief of Naval Operations
Department of the Navy
Washington, DC 20350-2000

29 Attn: J. Schuster (N87T)
30 CAPT M. Wachendorf (N874)

Office of the Chief of Naval Operations
Naval Observatory
34th and Massachusetts Ave. Northwest
Washington, DC 20390-1800

31 Attn: R. Winokur (Code OP-95)

Office of Naval Research
Department of the Navy
Arlington, VA 22217-5000

32 Attn: J. DeCorpo (Code 32)
33 S. Ramberg (Code 321)
34 J. Simmen (Code 321OA)
35 K. Dial (Code 321SS)
36 T. Goldsberry (Code 321US)
37 M. Shipley (Code 321US)
38 R. Doolittle (Code 321US)
39 R. Peloquin (Code 322OM)
40 B. Blumenthal (Code 322OM)

Advanced Research Projects Agency
3701 N. Fairfax Dr.
Arlington, VA 22203-1714

41 Attn: C. Stuart (MSTO)
42 W. Carey (MSTO)
43 T. Kooij (MSTO)
44 LCDR P. Feldman

Director
Naval Research Laboratory
4555 Overlook Avenue Southwest
Washington, DC 20375-5000

45 Attn: S. Wolf (7120)
46 E. Livingston (7121)
47 B. Palmer (5160)
48 B. Pasewark (7127)
49 M. Czarnecki (5110)
50 M. Collins (Code 5160)
51 W. Smith (Code 5582)

Distribution List for ARL-TR-94-18 under Contract N00039-91-C-0082,
TD No. 01A1030
(cont'd)

Copy No.

Commanding Officer
Naval Air Warfare Center
Aircraft Division, Warminster
Street and Jacksonville Roads
Warminster, PA 18974-5000

52 Attn: J. McEachern (Code 45C)
53 A. Horbach (Code 5031)

Officer in Charge
Naval Underwater Warfare Center
New London Detachment
New London, CT 06320-5594

54 Attn: N. Owsley
55 P. Herstein (3112)
56 R. Deavenport (Code 3332)

Director
Office of Naval Intelligence
4301 Suitland Rd.
Washington, DC 20395-5020

57 Attn: E. McWethy

58 Commanding Officer and Director
Defense Technical Information Center
Cameron Station, Building 5
5010 Duke Street
Alexandria, VA 22314

Director
North Atlantic Treaty Organization
SACLANT ASW Research Centre
APO New York 09019

59 Attn: Library
60 F. Jensen
61 D. Gingras
62 J. Fawcett

Marine Physical Laboratory
Scripps Institution of Oceanography
The University of California, San Diego
San Diego, CA 92132

63 Attn: F. Fisher
64 W. Hodgkiss
65 G. D'Spain
66 W. A. Kuperman

Distribution List for ARL-TR-94-18 under Contract N00039-91-C-0082,
TD No. 01A1030
(cont'd)

Copy No.

The Johns Hopkins University
Applied Physics Laboratory
Johns Hopkins Road
Laurel, MD 20723-6099

67 Attn: K. McCann
68 R. Mitnick
69 H. South

The Mitre Corporation
7525 Colshire Drive
McLean, VA 22102

70 Attn: K. Hawker
71 J. Hagy

Science Applications International Corporation
P.O. Box 1303
McLean, VA 22102

72 Attn: J. Hanna
73 R. Cavanagh

Center for Applied Mathematics and Statistics
New Jersey Institute of Technology
Newark, NJ 07102

74 Attn: M. B. Porter

75 Environmental Sciences Group, ARL:UT

76 Hans A. Baade, ARL:UT

77 Nancy R. Bedford, ARL:UT

78 Karl C. Focke, ARL:UT

79 Richard A. Gramann, ARL:UT

80 David E. Grant, ARL:UT

81 Jonathan H. Gross, ARL:UT

82 David P. Knobles, ARL:UT

83 Robert A. Koch, ARL:UT

84 Thomas N. Lawrence, ARL:UT

85 Fredrick W. Machell, ARL:UT

Distribution List for ARL-TR-94-18 under Contract N00039-91-C-0082,
TD No. 01A1030
(cont'd)

Copy No.	
86	Peter E. McCarty, ARL:UT
87	Clark S. Penrod, ARL:UT
88	Carol V. Sheppard, ARL:UT
89	Eric Smith, ARL:UT
90–99	Evan K. Westwood, ARL:UT
100	Library, ARL:UT
101	Reserve, Environmental Sciences Group, ARL:UT